DETONATION BRANCHING IN A PDE WITH LIQUID HYDROCARBON FUEL

THESIS

Kristin L. Panzenhagen, First Lieutenant, USAF

AFIT/GAE/ENY/04-M13

DEPARTMENT OF THE AIR FORCE
AIR UNIVERSITY

AIR FORCE INSTITUTE OF TECHNOLOGY

Wright-Patterson Air Force Base, Ohio

AFIT/GAE/ENY/04-M13

DETONATION BRANCHING IN A PDE WITH LIQUID HYDROCARBON FUEL

THESIS

Presented to the Faculty

Department of Aeronautics and Astronautics

Graduate School of Engineering and Management

Air Force Institute of Technology

Air University

Air Education and Training Command

In Partial Fulfillment of the Requirements for the

Degree of Master of Science in Aeronautical Engineering

Kristin L. Panzenhagen, BS

First Lieutenant, USAF

March 2004

AFIT/GAE/ENY/04-M13

DETONATION BRANCHING IN A PDE WITH LIQUID HYDROCARBON FUEL

Kristin L. Panzenhagen, BS
First Lieutenant, USAF

Approved:

//signed//	11 Mar 04
Paul I. King (Chairman)	date
//signed//	11 Mar 04
Ralph A. Anthenien (Member)	date
//signed//	11 Mar 04
Mark F. Reeder (Member)	date

Acknowledgments

I would like to thank my advisor, Dr. Paul King, for affording me the opportunity to do such interesting research. I would also like to thank Capt Colin Tucker who worked with me every step of the way and Drs. Fred Schauer and John Hoke who were always willing to share with me their PDE expertise. Also, thanks to Ted Williams and Joe Mantz who gave of their time and resources so I could run sparging experiments. Many thanks to Dwight Fox and Walt Balster for all the welding, drilling, cutting, bending and assembling that made the vaporization system possible and to Jeff Stutrud, the computer guru. I am especially indebted to Royce Bradley and Curt Rice who guided all my efforts in the lab. Most of all, I would like to thank the Lord for leading me to this assignment where I met my fiancé.

Kristin L. Panzenhagen

Table of Contents

List of Figures

Page

List of Tables

List of Symbols

Acronyms

CEA	calculation of complex chemical equilibrium compositions and applications
C-J	Chapman Jouguet
DDT	deflagration to detonation transition
GC	gas chromatograph
PDE	pulse detonation engine
TCD	thermal conductivity detector

Regular Symbols

A	control volume cross sectional area [m^2]
c	speed of sound [m/s]
c_p	constant-pressure specific heat [kJ/kgK]
$\overline{g}$	acceleration of gravity vector [m/s^2]
h	enthalpy [kJ/kg]
h_f°	enthalpy of formation [kJ/kg]
FN	flow number [$lbm/psia^{0.5}hr$]
k	thermal conductivity [W/mK]
$\dot{m}$	mass flow rate [kg/s]
$\dot{m}''$	mass flux [kg/m^2s]
M	Mach number [unitless]
MW	molecular weight [g/mol]
P	pressure [bar]
q	heat of combustion per mass [kJ/kg]
R	gas constant [kJ/kgK]
T	temperature [K]
t	time [s]
u	velocity [m/s]
$\overline{U}$	velocity vector with components in three directions [m/s]
Y	mass fraction [unitless]

Greek Symbols

δ_{ij}	Kronecker delta [unitless]
τ_{ij}'	viscous stresses [kg/km*s]
γ	specific-heat ratio [unitless]
λ	bulk viscosity coefficient [Pa*s]
μ	viscosity coefficient [Pa*s]
ρ	density [kg/m^3]

Subscripts

1	reactants
2	products
D	detonation
i	single species in the product or reactant
ref	reference point
sat	saturated
u	universal

Abstract

Pulse detonation engines (PDE) capitalize on the large mass flux and pressure rise a detonation has compared to a deflagration. The PDE operates on a fill-detonate-exhaust cycle and its thrust is directly proportional to the cycle frequency, therefore a decrease in cycle time results in increased thrust. This research showed that the detonate part of the cycle can be shortened by using a branched detonation as the ignition source as opposed to standard spark ignition. This research was a milestone in PDE development because, while detonation branching has been accomplished using gaseous hydrogen as the fuel, this was the first instance of detonation branching using liquid hydrocarbon fuel. A vaporization system was used to vaporize the fuel and mix it with the airstream, allowing the PDE to operate at stoichiometric conditions.

This research concluded that detonation ignition is not only possible when using liquid hydrocarbon fuel, but it produces results superior to those obtained using spark ignition. With detonation ignition, more energy is input into the head than with spark ignition. Operating at a 20 Hz cycle frequency and a 1.02 equivalence ratio, ignition times were 5.63 and 0.19 ms and deflagration to detonation transition (DDT) times were 2.36 and 1.03 ms for the spark- and detonation-ignited thrust tubes, respectively. The total time savings in the detonate part of the PDE cycle for detonation-ignition was 6.77 ms, an 85% time reduction in ignition and DDT times. This reduction in cycle time affords an appreciable thrust increase. Also, DDT was complete in 83% of the distance, allowing a decrease in tube length, which decreases overall weight.

DETONATION BRANCHING IN A PDE

WITH LIQUID HYDROCABRON FUEL

1 Introduction

1.1 General

Pulse detonation engine (PDE) development is of much interest in the propulsion world. PDEs are mechanically simple engines with the potential for high thrust in a large operational envelope, low weight, low cost and ease of scalability (Schauer et al., 2001:1).

This project's purpose was to use detonation branching as an ignition source in a PDE operating with a stoichiometric mixture of liquid hydrocarbon fuel and air. Detonation branching as an ignition source using hydrogen as the fuel is a proven concept (Rolling et al., 2002:7), as is using liquid hydrocarbon fuels in a PDE with spark ignition (Tucker et al., 2004:1). Combining the two concepts by using branched detonations as an ignition source in a PDE running on liquid hydrocarbon fuel has yet to be accomplished, and is the objective of this research.

The Air Force Research Laboratory Propulsion Directorate, Turbine Engine Division, Combustion Sciences Branch, Wright-Patterson AFB, Ohio and the Air Force Office of Scientific Research sponsored this project. The research was conducted in the Pulse Detonation Research Laboratory at Wright-Patterson AFB in Building 71's D-Bay test cell.

1.2 Background

To generate thrust using a detonation, a tube is closed at one end, filled with a combustible fuel-oxidizer mixture and ignited at the closed end. The combustion products between the flame and the closed end of the tube expand to five to fifteen times the specific volume of the reactants, sending compression waves ahead of the flame and accelerating the flame toward the open end of the tube (Glassman, 1996:223). Each compression wave raises the reactants' temperature, which increases the speed of sound and causes the compression waves to coalesce (Glassman, 1996:223). The coalescing compression waves form a shock wave that ignites the reactants ahead of the flame (Glassman, 1996:223). The shock wave coupled with the combustion region is the detonation. A detonation propagates at supersonic speeds and thrust is produced from the large momentum flux associated with the high product velocity (Schultz et al., 1999:1). Section 2.3 gives a more detailed description of detonation formation.

Before the detonation is formed, the combustion region is a deflagration that must transition to a detonation. The most notable differences between a deflagration and detonation are the flame speed and the pressure rise across the flame.

Figure 1.1 shows a flame propagating from right to left in a tube. In the figure, u_1 is the reactants' velocity with respect to the flame front, which is the same magnitude as the flame front velocity with respect to the stationary tube; u_2 is the products' velocity with respect to the flame front. Also, P is pressure, T is temperature, ρ is density, c is the speed of sound and M is the Mach number. The subscripts *1* and *2* indicate reactants and products, respectively. Table 1.1 uses a stoichiometric methane-air mixture with

standard pressure and temperature at the initial conditions to show how gas properties differ for detonations and deflagrations (Turns, 2000:600) based on Fig. 1.1.

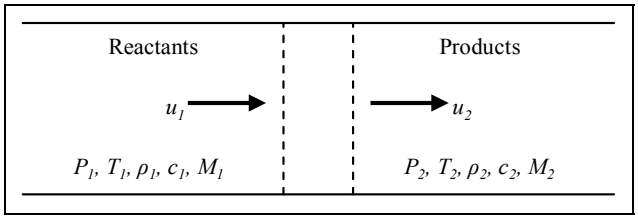

Fig. 1.1 Flame propagation from right to left

Table 1.1 Detonation and deflagration gas properties (Turns, 2000:600)

Property	Detonation	Deflagration
M_1	5 – 10	0.001
M_2	1	0.003
u_2/u_1	0.4 – 0.7	7.5
P_2/P_1	13 – 55	≈ 1
T_2/T_1	8 – 21	7.5
ρ_2/ρ_1	1.7 – 2.6	0.13

Comparing M_1 and M_2 in Table 1.1 for a detonation and deflagration shows a notable difference in flame Mach number. A standard detonation travels supersonically relative to the reactants and sonically relative to the products, while a standard deflagration is always subsonic. A detonation velocity is on the order of km/s, while a deflagration velocity is on the order of cm/s (Turns, 2000:254).

Comparing the values for P_2/P_1 in Table 1.1 shows the difference in the pressure rise across the flame for a detonation and deflagration. PDEs use a constant volume process which causes pressure to increase by an order of magnitude across a detonation. A deflagration occurs in a constant pressure process.

In a detonation, large velocities and pressures result in large mass fluxes and pressure differentials that create thrust (Schultz et al., 1999:1). Since a detonation has a

larger product velocity and pressure rise than a deflagration, it produces thrust more effectively. PDEs are designed to capitalize on a detonation's thrust producing ability.

Each detonation in a PDE consists of a three-part cycle: fill, detonate and exhaust, shown in Fig. 1.2. The first part fills the thrust tube with a detonable fuel-oxidizer mixture. The second part ignites the mixture to create a deflagration, transitions the deflagration to a detonation and propagates the detonation through the thrust tube. The third part allows the combustion products to exit the thrust tube.

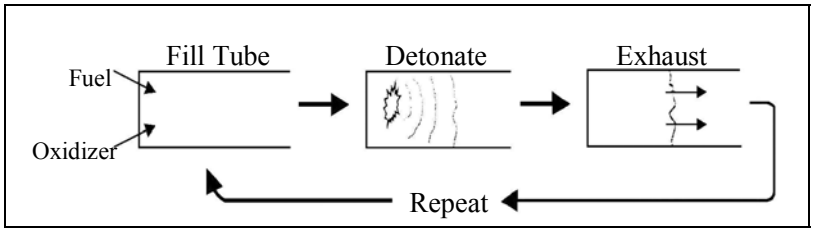

Fig. 1.2 Three-part PDE cycle

In a PDE, thrust is directly proportional to detonation frequency. One way increase thrust is to incorporate multiple thrust tubes into a PDE. Another way is to increase cycle frequency. To do this, the duration of at least one of the three parts of the PDE cycle must decrease. Typically, the fill and exhaust parts of the cycle operate with valving that has mechanical limitations. The detonate part of the cycle, including ignition and deflagration to detonation transition (DDT), is not mechanically limited and has significant time savings potential. The detonate part of the cycle is this research's focus.

1.3 Problem Statement

This research addresses two issues in PDE development. First, for practical application, PDEs must run efficiently on liquid aviation fuels (Schauer et al., 2001:2). Second, using a branched detonation as an ignition source is a faster, more efficient way to produce detonations than using a spark.

There are vaporization problems associated with using liquid fuel. Long mixing times and lengths are required for enough fuel to vaporize to create a combustible fuel-oxidizer mixture (Brophy et al., 2000:1). Even in a long mixing length, liquid fuel does not completely vaporize, which decreases the amount of fuel mixing with air to create a combustible mixture. Therefore, PDEs using liquid fuel must run fuel rich. Also, part of the ignition source energy is removed from the ignition process and used to vaporize the droplets (Tucker et al., 2004:1), resulting in increased ignition time.

Recent research used a high-pressure fuel vaporization system to completely vaporize liquid fuel and then allowed it to mix with air and form a homogeneous, gaseous, combustible mixture (Tucker et al., 2004:1). Using vaporized fuel increases PDE efficiency by allowing it to operate with a stoichiometric fuel-air mixture, as opposed to the fuel-rich mixture necessary when using fuel in the liquid state. The research presented in this paper uses a vaporization system to transform liquid hydrocarbon fuel to the vapor state.

The second issue addressed in this research is the cycle time-savings potential from using a non-standard ignition source to decrease ignition and DDT times. In detonation branching, a conventional ignition source, such as a spark plug, ignites the combustible mixture in the first thrust tube. A crossover tube is located downstream of the point where the detonation forms. As the detonation passes the crossover tube, part

of the detonation branches into the crossover tube and the rest proceeds down the thrust tube to produce thrust. The detonation in the crossover tube is branched into a second thrust tube where the hot exhaust gases behind the shock wave ignite the combustible mixture (Rolling et al., 2002:2).

A branched detonation has more energy than a standard ignition source, which causes ignition and DDT to occur more quickly (Tucker et al., 2003:3). Decreasing ignition and DDT time decreases overall cycle time, enabling higher firing frequencies accompanied by increased thrust.

1.4 Objectives

The objective of this research was to use vaporized liquid hydrocarbon fuel in a detonation branching PDE configuration. The following steps were accomplished.

1. Construct a vaporization system.
2. Determine the optimum system configuration for detonation formation using vaporized liquid fuel in a single-tube PDE configuration with spark plug ignition.
3. Install a crossover tube at the location of DDT completion.
4. Measure and compare ignition and DDT times in the spark- and detonation-ignited thrust tubes.

1.5 Chapter Summary

A PDE is a mechanically simple engine that has the potential to use detonations to create high thrust in a large operational envelope. A detonation produces more thrust

than a deflagration because it has more mass flux and a larger pressure rise. This research focuses on combining two areas of current PDE development. First, it improves the PDE's efficiency by using a vaporization system to vaporize liquid fuel, which allows the engine to use liquid fuel without the typical condensing and mixing issues. Second, it uses detonation branching as an ignition source, which decreases ignition and DDT times, consequently decreasing cycle frequency and increasing thrust.

2 Theory

2.1 Introduction

PDEs capitalize on a detonation's pressure rise and product velocity to generate thrust. This chapter begins by discussing ignition and DDT. Then detonation mechanics are developed using four theoretical models: the one-dimensional analysis; the detonation velocity model; the Zeldovich, von Neumann and Döring detonation wave model and the three-dimensional detonation wave structure model.

2.2 Ignition Delay

Ignition is the first step in the detonate portion of the three-part PDE cycle, shown in Fig. 1.2. It is desirable for ignition to occur quickly to minimize cycle time and consequently maximize thrust.

The ignition process begins with the introduction of a flame-causing external stimulus. The stimulus causes reactant gasses to undergo inert heating, mixing and reactions that culminate in ignition (Kuo, 1986:744). Ignition delay, also known as the induction period (Turns, 2000:186), is the time from the introduction of the flame-causing stimulus to the moment of sustained ignition (Kuo, 1986:744).

Ignition delay is governed by the reactants' formation of intermediate species and their ensuing reactions (Turns, 2000:188). In order to understand how to control ignition delay, it is important to note how the reactants and their thermodynamic conditions affect it. Ignition delay decreases with decreasing reactant heat capacity and increasing reaction rate temperature dependence, heat of combustion and initial reaction rate

(Kanury, 1975:94). It also decreases with increasing heat flux and pressure (Kuo, 1986:750).

2.3 Deflagration to Detonation Transition

In a PDE, it is desirable for DDT to occur quickly and in a short distance. Shortening DDT time decreases the detonate part of the cycle, allowing a frequency increase that is accompanied by a thrust increase. Shortening DDT distance decreases the necessary thrust tube length, resulting in weight savings, a consideration when designing any aeronautical propulsion device.

Unless otherwise noted, the DDT process is presented as outlined by Kuo (Kuo, 1986:267-271). DDT begins with a laminar flame front, outside of which is a region of turbulent flow (Lewis and von Elbe, 1961:546). The turbulence increases the flame front's surface area, causing the flame to accelerate through the combustible mixture (Lewis and von Elbe, 1961:546). The reacting flow field's expansion, thermal conduction and species transport also cause flame acceleration (Schultz et al., 1999:3).

The flame's acceleration generates compression waves ahead of it that serve two functions. First, they preheat and compress the reactants ahead of the flame front, which further accelerates the flame front (Lewis and von Elbe, 1961:546). Second, they coalesce to form a shock wave known as the superdetonation wave. The superdetonation wave causes motion in the reactants, forcing the flame behind the shock to become turbulent. Within the turbulent flame, pockets of reactants reach the ignition condition and ignite, a phenomenon known as an "explosion within an explosion", resulting in small blast waves that propagate and amplify (Schultz et al., 1999:3).

The superdetonation wave proceeds into the unburned reactants. A second shock wave, known as a retonation wave, proceeds in the opposite direction into the products. As the two shocks progress, they take on the appearance of a spherical shock originating at the explosion within an explosion.

Oscillations known as transverse waves develop between the two shock waves. The transverse waves react with the shocks, causing the forward moving shock to couple with the combustion zone. This shock-combustion coupling is the steady detonation.

2.4 One-Dimensional Analysis

In 1899, Chapman developed a one-dimensional detonation analysis (Turns, 2000:600). Although detonations are three-dimensional, Chapman's model provides the basic understanding needed before making a more complex detonation analysis.

Unless otherwise noted, the one-dimensional analysis development in this section is from Turns (Turns, 2000:600-605). Figure 2.1 shows the control volume and gas properties used in the analysis. In the figure, P is pressure, T is temperature, ρ is density, h is enthalpy and u is axial velocity. The subscripts *1* and *2* indicate reactants and products, respectively.

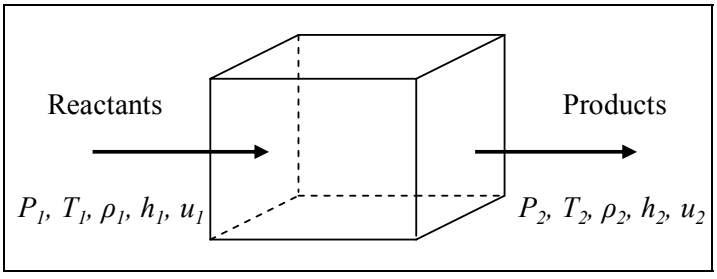

Fig. 2.1 Control volume in one-dimensional analysis

The one-dimensional analysis assumes one-dimensional, steady flow; constant area; ideal gas; constant and equal specific heats; negligible body forces and adiabatic conditions. The analysis begins with the conservation laws for the control volume. Equations 1, 2 and 3 give conservation of mass, momentum and energy, respectively (White, 1991:59-73). In these equations, t is time, $\overline{U}$ is the velocity vector, $\overline{g}$ is the acceleration of gravity vector, τ_{ij}' is viscous stresses and k is thermal conductivity. Equation 4 defines τ_{ij}', where μ is the viscosity coefficient, δ_{ij} is the Kronecker delta and λ is the bulk viscosity coefficient (White, 1991:73).

$$\frac{\partial \rho}{\partial t} + div\left(\rho \overline{U}\right) = 0 \qquad [1]$$

$$\rho \frac{D\overline{U}}{Dt} = \rho \overline{g} + \overline{\nabla} \cdot \tau_{ij}' - \overline{\nabla} P \qquad [2]$$

$$\rho \frac{Dh}{Dt} = \frac{DP}{Dt} + div\left(k \overline{\nabla} T\right) + \tau_{ij}' \frac{\partial u_i}{\partial x_j} \qquad [3]$$

$$\tau_{ij}' = \mu\left(\frac{\partial u_i}{\partial x_j} + \frac{\partial u_j}{\partial x_i}\right) + \delta_{ij} \lambda div \overline{U} \qquad [4]$$

Applying the assumptions for the one-dimensional analysis to Eqs. 1, 2 and 3 yields Eqs. 5, 6 and 7, the simplified conservation of mass, momentum and energy equations, respectively. In these equations, $\dot{m}$ is mass flow rate, A is cross sectional area and $\dot{m}'' = \dot{m}$ /A is mass flux.

$$\dot{m}'' = \rho_1 u_1 = \rho_2 u_2 \qquad [5]$$

$$P_1 + \rho_1 u_1^2 = P_2 + \rho_2 u_2^2 \qquad [6]$$

$$h_1 + \frac{u_1^2}{2} = h_2 + \frac{u_2^2}{2} \qquad [7]$$

Equation 8 gives the calorific equation of state, where Y is the mass fraction, h_f° is the enthalpy of formation and c_p is the constant-pressure specific heat. The subscript i indicates a single species in the product or reactant and the subscript *ref* indicates the reference point. Applying the assumptions for the one-dimensional analysis yields Eq. 9, the simplified equation of state.

$$h(T) = \sum Y_i h_{f,i}^\circ + \sum Y_i \int_{T_{ref}}^{T} c_{p,i} dT \qquad [8]$$

$$h(T) = \sum Y_i h_{f,i}^\circ + c_p \left(T - T_{ref}\right) \qquad [9]$$

Substituting Eq. 9 into the simplified energy conservation equation, Eq. 7, yields Eq. 10. Equation 11 defines q, the heat of combustion per mass of the gas mixture. The magnitude of q depends on the specific fuel-oxidizer combination used and the equivalence ratio.

$$c_p T_1 + \frac{u_{x,1}^2}{2} + q = c_p T_2 + \frac{u_{x,2}^2}{2} \qquad [10]$$

$$q = \sum_{state1} Y_i h_{f,i}^\circ - \sum_{state2} Y_i h_{f,i}^\circ \qquad [11]$$

Assumming the products and reactants behave as ideal gasses allows the ideal gas equation, Eq. 12, to be used. In Eq. 12, R is the specific gas constant, $R = R_u / MW$, where R_u is the universal gas constant and MW is the gas' molecular weight.

$$P = \rho R T \qquad [12]$$

Using the above conservations equations, Rayleigh lines, which are lines of constant mass flux, can be developed. Using Eqs. 5 and 6, mass flux is determined in terms of pressures and densities, as shown in Eq. 13. By fixing the reactant pressure and density, a Rayleigh line can be plotted on the axes of pressure versus specific volume, the inverse of density, for each mass flux. Figure 2.2 shows the Rayleigh lines, with A and B indicating regions that are physically impossible for the combustion wave to reach.

$$\frac{P_2 - P_1}{1/\rho_2 - 1/\rho_1} = -\dot{m}''^2 \qquad [13]$$

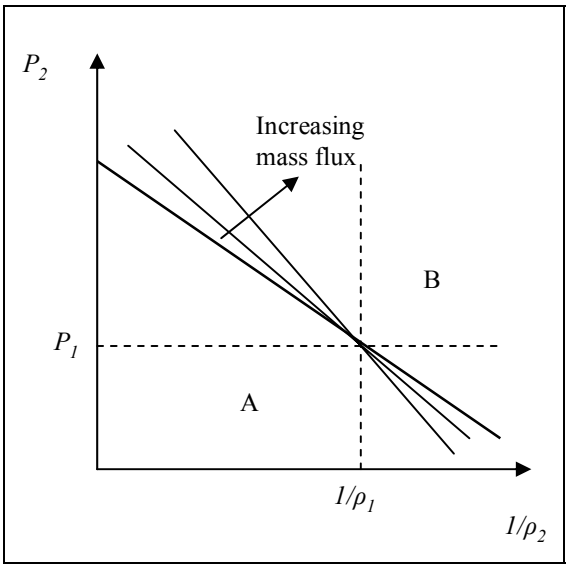

Fig. 2.2 Rayleigh lines

Equations 1 through 13 state conservation laws, the caloric equation of state, the ideal gas law and other relationships valid for ideal gasses. These equations develop the Rankine-Hugoniot curve, given by Eq. 14, where γ is the specific-heat ratio. The Rankine-Hugoniot curve shows all mathematically possible combinations of ρ_2 and P_2 for a given ρ_1, P_1 and q.

$$\frac{\gamma}{\gamma-1}\left(\frac{P_2}{\rho_2}-\frac{P_1}{\rho_1}\right)-\frac{1}{2}\left(P_2-P_1\right)\left(\frac{1}{\rho_1}+\frac{1}{\rho_2}\right)-q=0 \qquad [14]$$

Fixing P_1 and ρ_1 and inputting a known value q results in a plot of the Rankine-Hugoniot curve on the axes of pressure versus specific volume. Combining the Rayleigh lines with the Rankine-Hugoniot curve defines the pressure and density ranges at which detonations will occur in specific fuel-oxidizer mixtures.

Figure 2.3 shows the Rankine-Hugoniot curve and the limiting Rayleigh lines. Both sets of limiting Rayleigh lines, which are the straight, dashed lines, intersect at the point ($1/\rho_1$, P_1). The first set has one line with constant P_1 and one with constant $1/\rho_1$. The two lines in the second set are both tangent to the Rankine-Hugoniot curve, one at the upper Chapman-Jouguet (C-J) point and the other at the lower (Lewis and von Elbe, 1961:518).

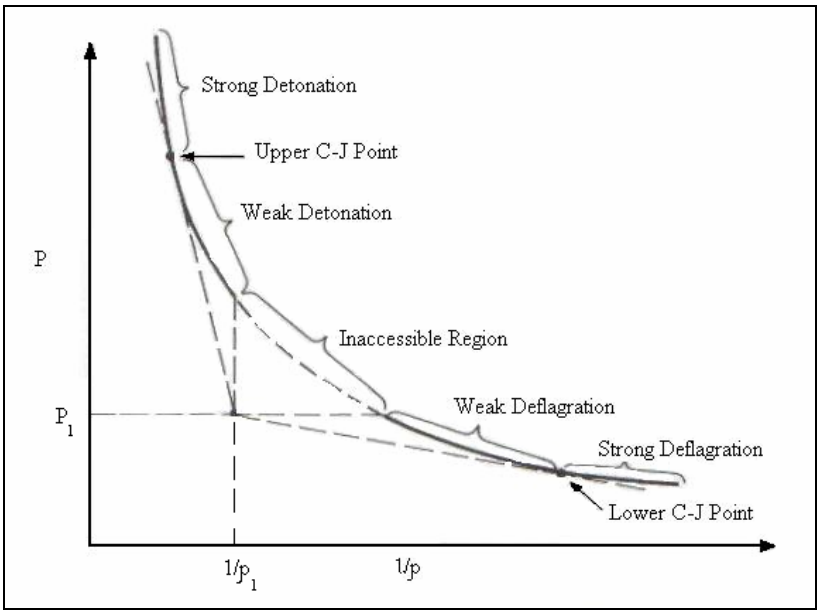

Fig. 2.3 Rankine-Hugoniot curve with limiting Rayleigh lines

The upper C-J point corresponds to a detonation state and is characterized by products with density and pressure exceeding that of the reactants (Kanury, 1975:275). At this point, products travel in the same direction as the detonation wave and with a velocity slower than that of the reactants (Kanury, 1975:275). PDEs are designed to operate at the upper C-J point.

The lower C-J point corresponds to a deflagration state and is characterized by products with density and pressure less than that of the reactants (Kanury, 1975:275). The products at the lower C-J point travel in the opposite direction as the flame front and with a velocity faster than the reactants (Kanury, 1975:275).

The section of the curve above the upper C-J point is the strong detonation region where the products' density and pressure exceed that of the C-J detonation wave (Kuo, 1986:240). Relative to the detonation wave, the reactants' velocity is supersonic and the products' is subsonic (Kuo, 1986:240). The strong detonation is rarely seen because it requires an overdriven shock (Kuo, 1986:241).

The section of the curve immediately below the upper C-J point is the weak detonation region where the products' pressure is less than at the upper C-J point (Kuo, 1986:241). Relative to the detonation wave, the reactants' velocity is supersonic and the products' is a lower supersonic value (Kuo, 1986:241). The weak detonation is rare because it requires reactants with faster-than-average chemical kinetics (Kuo, 1986:241).

In Fig. 2.3, the dashed section of the curve bounded by the constant $1/\rho_1$ and P_1 Rayleigh lines is a physically inaccessible region. This region is characterized by mass fluxes greater than infinity and less than zero, which are physically impossible (Kanury,

1975:274). In the physically inaccessible region, the velocity value is imaginary, which would require the compression wave to move backwards (Glassman, 1996:231).

The section of the curve immediately above the lower C-J point is the weak deflagration region where products' pressure, while slightly less than or equal to that of that of the reactants, is greater than that of the C-J deflagration wave (Kuo, 1986:242). The gas velocity relative to the deflagration wave increases but remains subsonic (Kuo, 1986:242). The weak deflagration is commonly observed in combustion-related experiments (Kuo, 1986:242).

The section of the curve below the lower C-J point is the strong deflagration region where the products' pressure is less than that of the C-J deflagration wave (Glassman, 1996:233). The gas velocity relative to the deflagration wave is accelerated from subsonic to supersonic (Kuo, 1986:242). The deflagration wave structure does not physically allow acceleration from subsonic to supersonic velocities in a constant area duct, therefore the strong deflagration is never observed experimentally (Kuo, 1986:242).

2.5 Detonation Velocity

The detonation velocity, u_D, is the velocity of the reactants relative to the detonation wave, denoted as u_1 in Fig. 2.1. Unless otherwise noted, the development of the detonation velocity presented in this section is from Turns (Turns, 2000:609-610). With the additional assumption that the products' pressure is much greater than the reactants', $P_2 >> P_1$, the one-dimensional analysis is used to determine the detonation

velocity. According to Table 1.1, the pressure increase across the combustion wave is an expected detonation characteristic.

To begin the velocity analysis, the one-dimensional conservation of mass equation, Eq. 5, is rewritten where the product velocity is at the upper C-J point. At this point, the product velocity is sonic and the speed of sound is $\sqrt{\gamma RT}$. Solving for the reactant velocity yields Eq. 15.

$$u_1 = \frac{\rho_2}{\rho_1}\sqrt{\gamma R_2 T_2} \qquad [15]$$

Applying the assumption that $P_2 >> P_1$ allows all P_1 terms in the one-dimensional momentum conservation equation, Eq. 6, to be neglected. Also, as with the mass conservation equation, $\sqrt{\gamma R_2 T_2}$ can be substituted for product velocity in the momentum conservation equation. Rearranging yields Eq. 16 and substituting Eq. 15 into Eq. 16 yields Eq. 17.

$$\frac{\rho_1 u_1^2}{\rho_2 \gamma R_2 T_2} - \frac{P_2}{\rho_2 \gamma R_2 T_2} = 1 \qquad [16]$$

$$\frac{\rho_2}{\rho_1} = 1 + \frac{P_2}{\rho_2 \gamma R_2 T_2} \qquad [17]$$

Substituting the ideal gas law, Eq. 12, into Eq. 17 yields the final transformation of the mass conservation equation for the detonation velocity analysis, Eq. 18.

$$\frac{\rho_2}{\rho_1} = \frac{\gamma + 1}{\gamma} \qquad [18]$$

The energy conservation equation from the one-dimensional analysis, Eq. 7, can also be transformed for use in the detonation velocity analysis. Substituting the speed of

sound for the product velocity and solving for the product temperature yields Eq. 19. Substituting Eq. 15 into Eq. 19 yields Eq. 20. Substituting Eq. 18 into Eq. 20 yields Eq. 21.

$$T_2 = T_1 + \frac{u_1^2 - \gamma R_2 T_2}{2c_p} + \frac{q}{c_p} \qquad [19]$$

$$T_2 = T_1 + \frac{\gamma R_2 T_2 \left(\left(\frac{\rho_2}{\rho_1} \right)^2 - 1 \right)}{2c_p} + \frac{q}{c_p} \qquad [20]$$

$$T_2 = T_1 + \frac{\gamma R_2 T_2 \left(\left(\frac{\gamma + 1}{\gamma} \right)^2 - 1 \right)}{2c_p} + \frac{q}{c_p} \qquad [21]$$

Applying the specific heat relation $\gamma - 1 = \frac{\gamma R}{c_p}$ (White, 1991:43) to Eq. 21 and solving for the product temperature yields the final transformation of the energy conservation equation for the detonation velocity analysis, Eq. 22.

$$T_2 = \frac{2\gamma^2}{\gamma + 1} \left(T_1 + \frac{q}{c_p} \right) \qquad [22]$$

To solve for the detonation velocity, the transformed versions of the mass and energy conservation equations, Eqs. 18 and 22, respectively, are substituted into Eq. 15, where the reactant velocity, u_1, is the detonation velocity, u_D. The result is Eq. 23. It is important to note that this equation is based on the assumptions from the one-dimensional analysis and the assumption that $P_2 >> P_1$.

$$u_1 = u_D = \sqrt{2(\gamma + 1)\gamma R_2 \left(T_1 + \frac{q}{c_p} \right)} \qquad [23]$$

Two methods for determining detonation wave speed using iterative techniques are the trial-and-error method and the Newton-Raphson method. The trial-and error method assumes P_2 and T_2 as a starting point and the Newton-Raphson method assumes P_2/P_1 and T_2/T_1 as a starting point (Kuo, 1986:252-258).

2.6 Zeldovich, von Neumann and Döring Detonation Wave Model

Independently, Zeldovich, von Neumann and Döring developed the same theory for the detonation wave structure, called the ZND detonation wave model (Kuo, 1986:261). The development of the ZND detonation wave model presented in this section is from Kuo (Kuo, 1986:261-262) unless otherwise noted. Assuming steady, one-dimensional flow, Zeldovich, von Neumann and Döring determined that a detonation is a shock wave with a thickness of several mean free paths, immediately followed by a much thicker area where chemical reactions occur. The shock wave travels through the reactants at the detonation velocity, but does not have sufficient thickness for chemical reactions to occur within it. As the shock wave travels through the reactants, it heats them to a temperature that allows them to react fast enough to produce a combustion wave that travels at the same rate as the shock wave, resulting in the shock-combustion coupling that is a detonation.

The ZND detonation wave structure consists of three regions: a shock wave, an induction zone and a reaction zone. The shock wave is a thin region with a sharp increase in pressure, temperature and density. The pressure increase is known as the von Neumann spike In the induction zone, which immediately follows the shock wave, the reaction rate slowly increases, as determined by the Arrhenius law (Kanury, 1975:28),

and the temperature, pressure and density are relatively constant. Following the induction zone is the reaction zone where the reaction rate sharply increases, resulting in a temperature increase and a pressure and density decrease. The reaction zone ends where the temperature, pressure and density reach equilibrium. The entire detonation wave is approximately 1 cm thick. Figure 2.4 shows the ZND model and its associated thermodynamic properties.

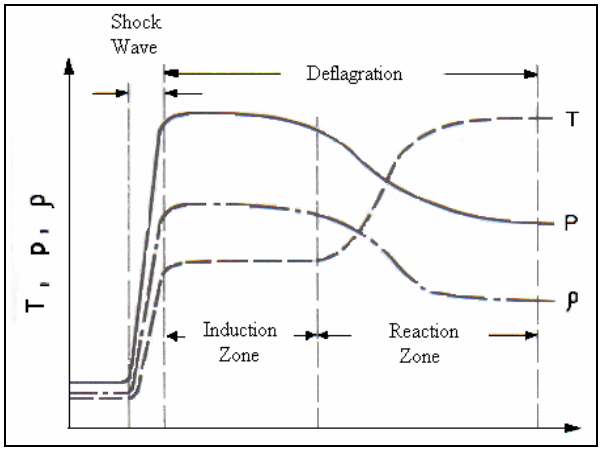

Fig. 2.4 ZND detonation wave structure and thermodynamic properties

2.7 Three-Dimensional Detonation Wave Structure

The one-dimensional analysis and the ZND detonation wave structure provide a foundation for understanding detonations with the simplifying assumption that detonations are one-dimensional. In reality, however, detonations are highly three-dimensional.

In 1959, Denisov and Troshin proved three-dimensional propagation is a characteristic of all detonation waves (Kuo, 1986:263). They passed a detonation along soot-coated foil and the detonation "wrote" on the foil, showing that it not only traveled

parallel to the foil, but also had a velocity component perpendicular to it (Kuo, 1986:263-265).

The "writing" on the foil shows the intersection of three shock waves: Mach-stem, incident and reflected (Kuo, 1986:264). The intersection, known as the triple point, has shear discontinuities around it (Glassman, 1996:254), called slip lines (Shapiro, 1953:555). The slip lines are thin regions of concentrated vorticity that appear as surface discontinuities (Shapiro, 1953:555). The slip lines push the soot away and cause it to build up along the triple point (Glassman, 1996:254-255). The lines on the foil outline the trajectory of the triple points and form enclosed regions known as cells (Glassman, 1996:255). Figure 2.5 shows the schematic diagram of the foil record of a detonation proceeding from left to right, with A, B, C and D representing triple points.

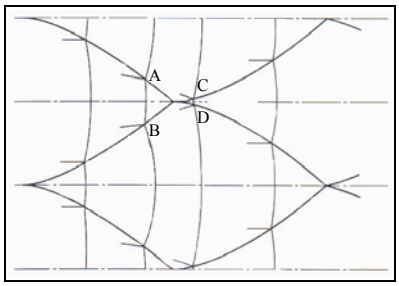

Fig. 2.5 Diagram of smoke foil record of detonation moving left to right

The cells record the cyclic nature of the detonation wave front. The front of each cell shows an overdriven shock with a velocity of about 1.6 times C-J detonation velocity (Glassman, 1996:255). The rest of the cell shows the decay of the shock until it reaches about 0.6 times C-J detonation velocity (Glassman, 1996:255). Then, transverse waves collide, returning the wave front to the overdriven state and the cycle repeats (Glassman, 1996:255). The average velocity is the C-J detonation velocity.

2.8 Chapter Summary

Two events in the firing portion of the three-part PDE cycle with the potential for time-savings are ignition and DDT. In ignition, a flame-causing external stimulus causes reactant gasses to undergo inert heating, mixing and reactions that culminate in ignition. In DDT, a flame accelerates through the combustible mixture, generating compression waves ahead of it that coalesce to form a shock wave. Eventually, the shock wave and combustion zone couple to form a detonation.

To understand detonation limits, Rayleigh lines, which are lines of constant mass flux, are used with the Rankine-Hugoniot curve, which shows all mathematically possible combinations of ρ_2 and P_2 for a given ρ_1, P_1 and q. The Rayleigh lines define C-J detonation and deflagration points as well as regions of strong and weak detonations, physically inaccessibility and weak and strong deflagrations on the Rankine-Hugoniot curve. PDEs are designed to operate at the C-J detonation point. The Rayleigh lines, Rankine-Hugoniot curve and C-J detonation velocity are developed using a one-dimensional approach, but it is important to note that detonations are highly three-dimensional.

3 Materials and Method

3.1 Introduction

This chapter describes the experimental setup used in this research to include fuel selection, the vaporization system, the PDE and surface deposit prevention. Error sources are also presented.

3.2 Fuel Selection

This research's goal is to branch detonations using vaporized liquid hydrocarbon fuel. Potential fuel choices were n-hexane (C_6H_{14}), n-heptane (C_7H_{16}) and isooctane (C_8H_{18}). In previous PDE research using the vaporization system, n-heptane had short DDT times and detonation speeds consistently at or above the C-J detonation velocity (Tucker et al., 2004:1), making it an appropriate fuel choice for this detonation branching research.

3.3 Vaporization System

The vaporization system's purpose is to convert fuel from a liquid state to a completely gaseous state, allowing the PDE to use a stoichiometric fuel-air mixture. Without the vaporization system, the PDE would require a fuel-rich mixture to overcome vaporization, mixing and recondensing problems encountered with liquid fuel. Figure 3.1 shows heptane's liquid-vapor dome to illustrate the state changes occurring in the vaporization system.

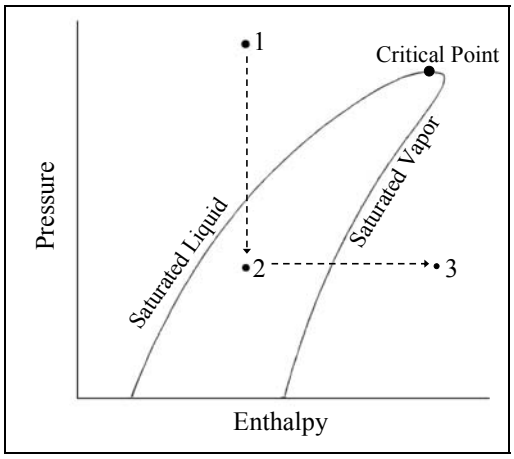

Fig. 3.1 Liquid-vapor dome showing heptane phase changes in the vaporization system

Liquid heptane enters the vaporization system at room temperature and is pressurized to 40 bar. Heptane's critical pressure and temperature are 27 bar and 540 K, respectively. Pressurizing above 27 bar prevents boiling when the fuel is heated. The pressurized heptane is heated to at least 420 K, indicated by point 1 in Fig. 3.1.

Then, the heptane is injected into the airstream through an adiabatic process in which enthalpy remains constant, but pressure drops to that of the airstream. The typical airstream pressure for one complete cycle, measured at the manifold, is shown in Fig. 3.2. At 1.8 bar, the lowest pressure in the vaporization system, the fuel is at 392 K, indicated by point 2 in Fig. 3.1. At this point, the fuel is inside the liquid-vapor dome.

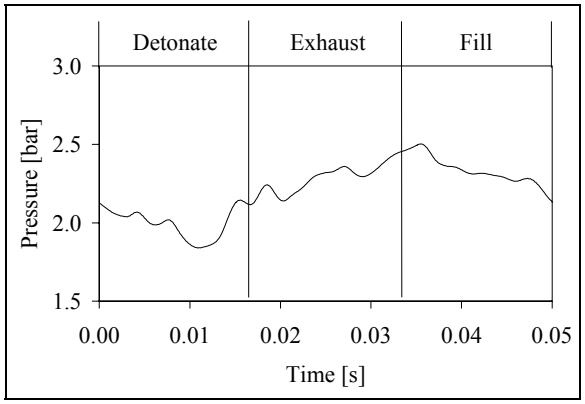

Fig. 3.2 One complete cycle of manifold airstream pressures without combustion

The injection temperature of 420 K is not sufficient for heptane to vaporize immediately upon injection. For immediate vaporization, the enthalpy of the saturated liquid fuel upstream of the injection point combined with the enthalpy of formation must be greater than or equal to the enthalpy of the saturated fuel vapor downstream of the injection point once it is at equilibrium with the airstream pressure, shown in Eq. 24.

$$h_{sat\ liquid,upstream} + h_{fg} \geq h_{sat\ vapor,downstream} \quad [24]$$

Equation 25 shows the energy balance used to determine the air and fuel temperatures that would cause fuel in the liquid state to vaporize upon mixing with the airstream and fuel in the vapor state to remain vapor.

$$\dot{m}_{mixture} c_{p,mixture} T_{mixture} = \dot{m}_{air} c_{p,air} T_{air} + \dot{m}_{fuel} c_{p,fuel} T_{fuel} \quad [25]$$

In Eq. 25, fuel in the fuel-air mixture is completely vapor. The National Institute of Standards and Technology computer program SUPERTRAPP Version 3.1 (Huber, 2003) defined $T_{mixture}$ for a 100% vaporous stoichiometric heptane-air mixture at equilibrium for various pressures, shown in Fig. 3.3. For pressures less than or equal to 3 bar, the fuel-air mixture is purely vapor at temperatures greater than or equal to 295 K.

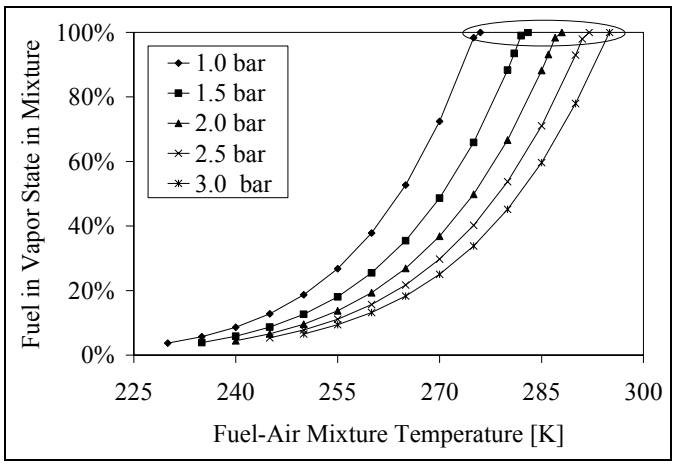

Fig. 3.3 Percent of heptane in vapor state in a stoichiometric fuel-air mixture

Equations 24 and 25 were solved for T_{air} and T_{fuel} and plotted to determine the operating envelope in which the fuel-air mixture would be purely vapor. Figures 3.4 and 3.5 show the results with the airstream at 1.5 and 3 bars, respectively. In the figures, the dashed line is from Eq. 24 and the solid line is from Eq. 25. The dot is the fuel and air temperatures just downstream of the injector in the PDE experiments.

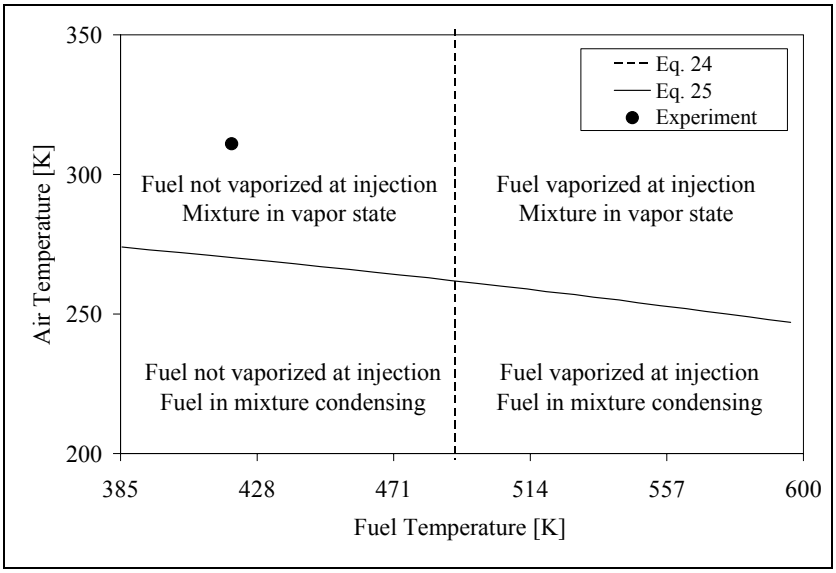

Fig. 3.4 Fuel and air temperature operating envelope, 1.5 bar airstream

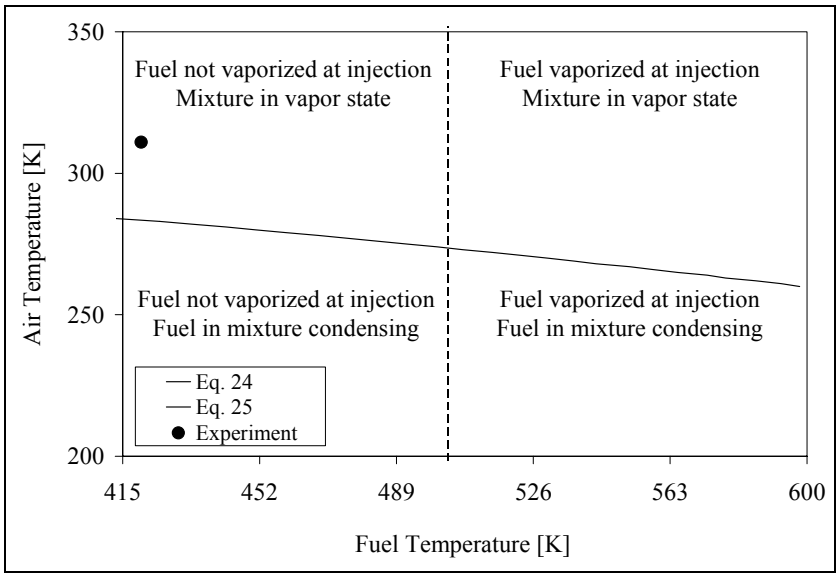

Fig. 3.5 Fuel and air temperature operating envelope, 3.0 bar airstream

Heptane is vaporized upon injection at temperatures greater than 490 and 514 K for pressures of 1.5 and 3.0 bar, respectively, as indicated by the vertical lines in Figs. 3.4 and 3.5. Heptane is entirely vapor in the stoichiometric fuel-air mixture at any point above the diagonal lines in Figs. 3.4 and 3.5. In this research, the fuel is not a vapor at injection, but vaporizes when mixed with the airstream, as indicated by the "Experiment" points on Figs. 3.4 and 3.5. Point 3 in Fig. 3.1 indicates this entirely vaporous state.

The vaporization system meets the temperature and pressure criteria described above to ensure vaporization upon mixing. Figure 3.6 shows a schematic of the complete vaporization system and the PDE thrust tubes. The fuel, air and fuel-air mixture temperatures and pressures are noted at various stages in the system.

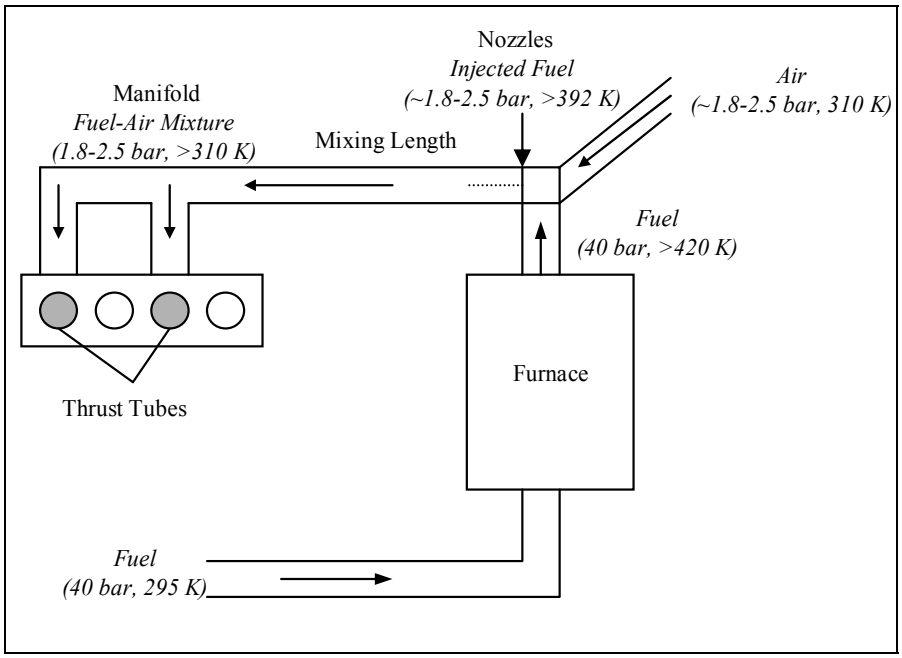

Fig. 3.6 Vaporization system schematic with temperatures and pressures

In the vaporization system, room temperature fuel is pressurized to 40 bar and fed into a reservoir in a furnace. The reservoir, shown in Fig. 3.7, consists of a vertical cylinder with tubing coiled around it. The cylinder is stainless steel Schedule 80 with a

0.48 m internal height and a 5 cm internal diameter. The tubing is stainless steel with a 13.72 m length and a 5 mm inner diameter. Combined, the cylinder and the tubing hold 1.2 L of fuel. The furnace heats the fuel in the reservoir to between 420 and 500 K.

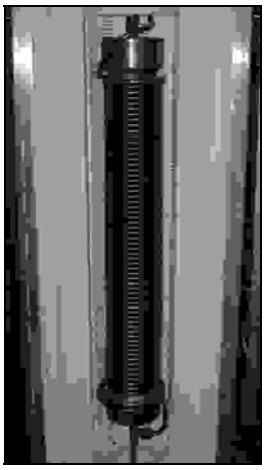

Fig. 3.7 Furnace fuel reservoir

From the furnace, the fuel flows through a fuel line, a valve and a flexible fuel line to the point where it is injected into the airstream. The fuel lines and valve are wrapped in heater tape, shown in Fig. 3.8, and woven fiberglass insulation to prevent the fuel from cooling before injection into the airstream. Just upstream of injection into the airstream, the fuel is at 40 bar with a temperature between 420 and 500 K.

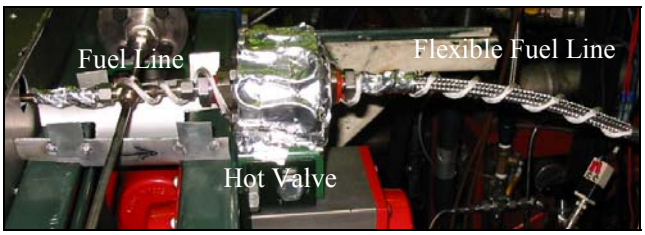

Fig. 3.8 Heater tape on fuel lines and hot valve

From the flexible fuel line, three pressure atomizing fuel nozzles inject the fuel into an airstream at 310 K. Fig. 3.9 shows one of the nozzles. A stock of variously sized nozzles allows the fuel flow rate to be changed for different test configurations.

Fig. 3.9 Fuel nozzle

The nozzles were categorized by their flow number (FN), defined in Eq. 26 where $\dot{m}$ is the desired fuel mass flow rate in lbm/hr, p_{fuel} is the pressure of the vaporized fuel in psig, ρ_{cal} is the calibrated density for heptane and ρ_{fuel} is the density of the fuel in the furnace in lbm/ft^3. The flow number for the experimental configuration was 3.45, as calculated in Appendix A. Three nozzles with a cumulative flow number as close as possible to 3.45 were used, resulting in an actual FN of 3.60.

$$FN = \frac{\dot{m}_{fuel}}{\sqrt{p_{fuel}}} \sqrt{\frac{\rho_{cal}}{\rho_{fuel}}} \qquad [26]$$

When fuel is injected into the airstream, its enthalpy remains constant while its pressure drops. Energy is used to convert part of the fuel to vapor as it drops from the liquid region in Fig. 3.1 to inside the liquid-vapor dome. To maintain constant enthalpy while using energy for the state change, the fuel temperature decreases slightly. The lowest fuel temperature immediately downstream of the nozzles is 392 and corresponds to a pressure of 1.8 bar.

The air is heated to 310 K by a 15 kW resistance heater with a tubular heating element for low pressure drop. As fuel mixes with the air, $T_{mixture}$ rises above the air temperature which ensures an entirely vaporous fuel-air mixture, according to Fig. 3.3.

The fuel-air mixture flows through 4.9 m of mixing length comprised of 0.1 m of stainless steel pipes, 0.3 m of mild steel pipes, 4.3 m of reinforced flexible tubing and a

0.2 m static mixing device, all with a 6.4 cm inner diameter. Figure 3.10 shows the mixing length.

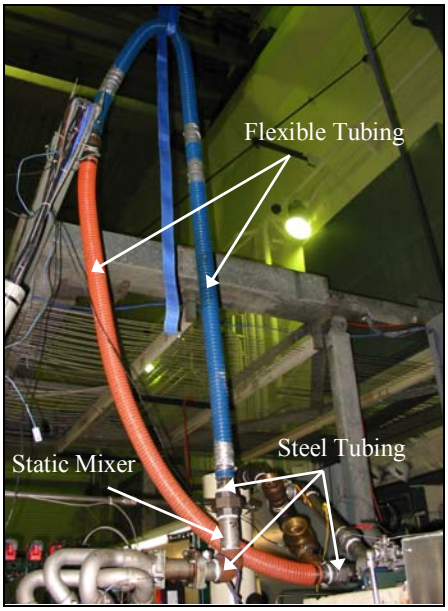

Fig. 3.10 Mixing length

Since the fuel is not entirely vapor prior to traveling through the mixing length, there is most likely some fuel dropout in the mixing length. This means the fuel-air mixture equivalence ratio in the PDE is slightly lower than the equivalence ratio determined by the amounts of fuel and air input into the vaporization system.

The fuel-air mixture temperature is monitored in the mixing length 0.16 m upstream from the manifold to ensure it does not fall below 310 K. This gives a 5% safety margin above 295 K, the minimum temperature for an entirely vaporous heptane-air mixture at 3 bar according to Fig. 3.3. After mixing, the fuel-air mixture flows into the manifold where the pressure varies from 1.8 to 2.5 bar, shown in Fig. 3.2. Figure 3.11 shows the manifold, which feeds the fuel-air mixture into four thrust tube heads.

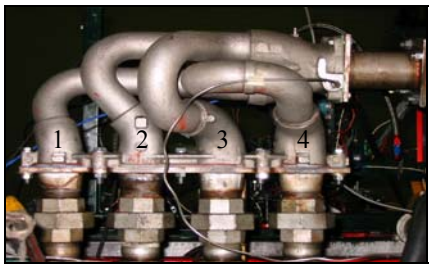

Fig. 3.11 Manifold that feeds fuel-air mixture into four thrust tube heads

Valves between the manifold and heads, shown in Fig. 3.12, control the flow rates into the heads. In this research, the PDE only uses thrust tubes 1 and 3, so valves 2 and 4 are closed. When valves 1 and 3 are fully open, valve 1 allows more mass flow than valve 3. To match flow rates, valve 1 is partially closed and valve 3 is completely open.

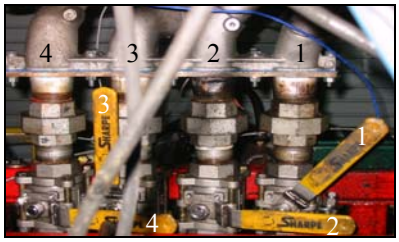

Fig. 3.12 Manifold and valves leading into thrust tube heads

From the manifold, the vaporization system interfaces with the PDE and the fuel-air mixture is fed into the thrust tube heads in accordance with the fill-detonate-exhaust cycle. The two thrust tubes used in this research are shown in Fig. 3.13.

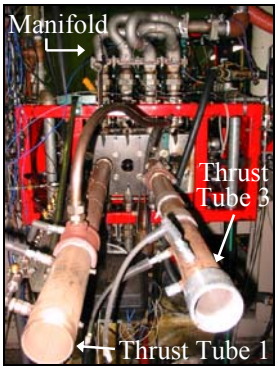

Fig. 3.13 Two thrust tubes

3.4 Pulse Detonation Engine

As discussed in Chapter 1, the PDE runs on a fill-detonate-exhaust cycle. In the PDE used in this research, each of the cycle's three parts are the same length. The fill and exhaust phases use valving from a General Motors Quad 4, Dual Overhead Cam cylinder head (Schauer et al., 2001:3). An electric motor drives the overhead cams and is capable of operating at up to 50 Hz (Schauer et al., 2001:3). The motor opens two ports during the fill cycle to allow the fuel-air mixture into the thrust tube and then opens two different ports during the exhaust cycle to allow cold air into the thrust tube to purge the remnants of the detonation process from the tube.

During the fill part of the PDE cycle, the fill fraction is 1.0, meaning 100% of the thrust and crossover tube volume is filled with fuel-air mixture so the detonation can travel the full length of the tubes. During the exhaust part of the cycle, the fill fraction is 0.5, meaning 50% of the thrust tube volume is filled with purge air. The purge air forces hot combustion products half way down the tube, so they will be completely expelled when the fuel-air mixture fills the tube, as shown in Fig. 3.14. Expelling the hot combustion products prevents unintentional ignition when the tube is filled with reactants and cools the tube walls (Schauer et al., 2001:4).

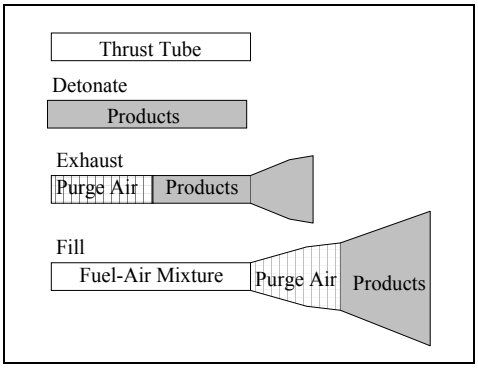

Fig. 3.14 Products being pushed out of thrust tube by purge air and fuel-air mixture

The cycle frequency and the amount of fuel-air mixture needed to fill the thrust and crossover tubes determine the fuel-air mass flow rate. The desired equivalence ratio is used to determine how much of the fuel-air mass flow needs to be fuel and how much needs to be air. Orifice plates in the air system downstream from the fuel injection point are sized to meter the air flow in the same way that fuel nozzles offer large scale fuel flow control. Varying the pressures that drive the fuel and air flows gives the exact mass flow to match the desired equivalence ratio.

The PDE has a 1.22 m thrust tube with a 5.5 cm inner diameter, a 1.22 m thrust tube with a 5.6 cm inner diameter and a 1.22 m crossover tube with a 1.7 cm inner diameter. To decrease DDT times by increasing hot spots and turbulence in the fuel-air mixture, each thrust tube has a 0.91 m Shelkin-like spiral, shown in Fig. 3.15.

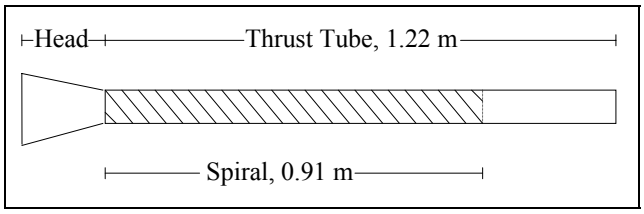

Fig. 3.15 Shelkin-like spiral in thrust tube

The first thrust tube's ignition source is a spark plug that uses capacitance discharge to create 105-115 mJ sparks (Tucker et al., 2004:4). The 20 Hz cycle frequency allows 3 ms for sparking, enough time for three sparks to be deposited into the head of the first thrust tube. The second thrust tube's ignition source is the detonation branched from the first tube and deposited into the second tube's head via the crossover tube. Figure 3.16 shows the thrust and crossover tubes.

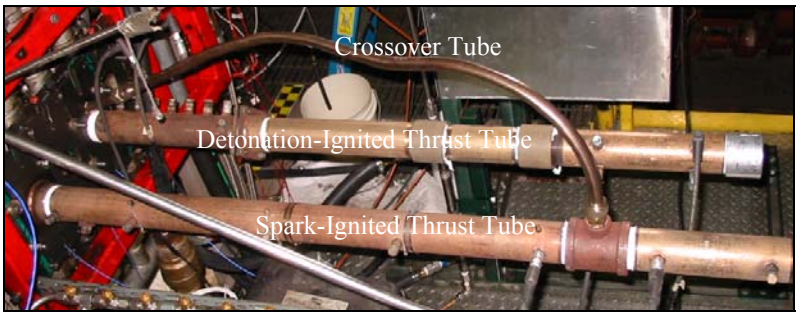

Fig. 3.16 Thrust tubes and crossover tube

A detailed description of the PDE's components and the systems used to control it is given by Schauer (Schauer et al., 2001:2-5).

Pressure transducers and homemade ion sensors take measurements during the detonation process to provide information about ignition and DDT times and detonation velocities and strengths. The model 102M232 pressure transducers are made by PCB Piezotronics. They are in the thrust tube heads and capture pressure rises associated with ignition and detonation.

The ion sensors are made from NGK spark plugs, model C-9E, part 7499. As combustion waves cross the ion sensors, they complet circuits and the sensors register voltage drops representing current flow. Ion sensors are positioned along the thrust and crossover tubes where combustion wave velocity readings are desired.

3.5 Carbon Deposit Prevention

When heated above 450 K (Heneghan et al., undated:3), dissolved molecular oxygen in fuel forms free radicals, causing hydrocarbon autoxidation reactions (Darrah, 1988:1). This thermal decomposition results in particulates (Ervin et al., 1998:1) and carbonaceous deposits on metal surfaces in fuel systems, a phenomenon known as coking

(Darrah 1988:1). The deposit amount varies linearly with the amount of oxygen in the fuel (Heneghan et al., undated:4) and increases with increasing fuel temperature (Ervin et al., 1998:3).

Since the vaporization system relies on fuel temperatures between 420 and 500 K, the potential exists for coking in fuel lines and nozzles. With the small nozzle and fuel line diameters, even a small amount of coking can reduce fuel flow.

When the oxygen content in fuel is less than 1 ppm, decomposition from dissolved oxygen is negligible (Darrah, 1988:1), so coking is minimal (Doungthip et al., 2002:2). With less than 1 ppm of dissolved oxygen, fuel can be heated to approximately 755 K before surface deposits form (Ervin et al., 1998:6). Lowering the fuel's oxygen content to less than 1 ppm before flowing it into the vaporization system ensures deposits will not clog the lines and nozzles.

In nitrogen sparging, nitrogen bubbles up through the fuel to displace oxygen in the fuel and ullage, which is vented out of the fuel container. Sparging experiments were performed to determine the amount of nitrogen needed to decrease dissolved oxygen below 1 ppm. N-hexane and isooctane were used in the experiments because the fuel to be used in the detonation branching research had yet to be determined.

In the sparging experiments, the thermal conductivity detector (TCD) in a Hewlett Packard 5890 Series II Gas Chromatograph (GC) measured oxygen dissolved in the fuel. The GC vaporizes and separates the oxygen in a fuel sample, the TCD passes the vapor over a filament in a circuit and measures the resistance, which is amplified, conditioned and plotted versus separation time (FVCC, 2004). On the plot, the area under the curve indicates the amount of dissolved oxygen in the fuel (FVCC, 2004).

The fuel tank in the sparging experiments was the Alloy Products Corp 18.9 L pressurized transfer tank used to sparge and hold the fuel in the detonation branching PDE research. The sparging line was a tube coiled around the bottom of the tank with holes drilled on top of it, shown in Figs. 3.17 and 3.18. The tank is at atmospheric pressure during sparging.

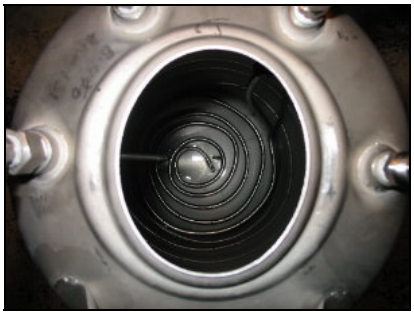

Fig. 3.17 Sparging coil in fuel tank

Fig. 3.18 Sparging coil close-up

Oxygen concentration in the ullage is denser than in the fuel, so more ullage increases the nitrogen needed to completely displace oxygen from the fuel tank. In the sparging experiments, the tank was filled with 11.0 L of fuel, leaving 7.9 L of ullage, to make the sparging more difficult than if the tank was completely full of fuel.

Air at 4.1 bar bubbled up from the coil for 5 min to saturate the fuel with oxygen so the GC could take baseline saturation readings. The baseline oxygen saturation reading corresponds to 65 to 80 ppm of oxygen by weight, the typical amount of oxygen in oxygen-saturated fuel (Striebich and Rubery, 1994:49). For the fuel to have less than 1 ppm oxygen, it must have 1.3 to 1.5% of the oxygen it contained at saturation. Fuel was considered deoxygenated when the GC reading of the area under the oxygen curve was less than 1.3% of the baseline saturation reading.

Nitrogen at 4.1 bar was sparged through the fuel and GC readings were taken periodically until the GC was unable to detect oxygen in the fuel, which was below 1.3%

of the saturation reading. Figure 3.19 shows the amount of oxygen in n-hexane and isooctane versus the amount of nitrogen used in sparging. Table 3.1 shows the nitrogen flow rate, sparging duration and total amount of nitrogen used to deoxygenate the fuels. As long as the sparging coil covers most of the fuel tank's bottom, the nitrogen flow rate does not affect the amount of nitrogen needed to deoxygenate the fuel.

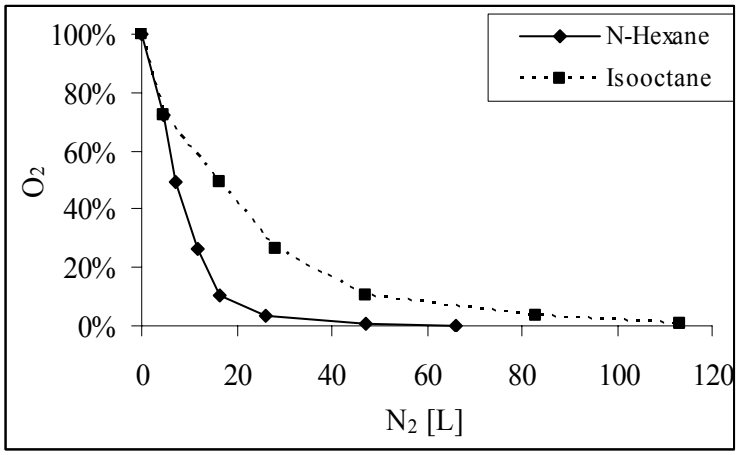

Fig. 3.19 Oxygen in n-hexane and isooctane versus nitrogen used in sparging

Table 3.1 Nitrogen used to sparge n-hexane and isooctane to less than 1 ppm of oxygen

Fuel	N_2 Flow [L/hr]	Time [min]	Total N_2 [L]
N-Hexane	142	28	66.1
Isooctane	142	48	113.3

The n-heptane used in the PDE research was sparged with the same amount of nitrogen as the isooctane in the sparging experiment, using 113.3 L of nitrogen per 11.0 L of n-heptane. Frequent nozzle inspections revealed no deposits, indicating this is a sufficient amount of nitrogen to sparge n-heptane.

3.6 Surface Coating

The second method of preventing deposits is surface treatment. Silcosteel® coating prevents impurities in the metal from reacting with fuel as hot as 673 K (Restek Corporation, 2003). The coiled tubing in the furnace is Silcosteel® coated stainless steel tubing. The rest of the tubing, fittings and nozzles in and directly downstream of the furnace are treated with Silcosteel®-AC coating (Restek Corporation, 2003).

The coating is thin enough, on the order of hundreds of Angstroms (Restek Corporation, 2003), to cause a negligible decrease in fuel line and nozzle cross-sectional area. Therefore, the nozzle flow number and flow pattern were not reexamined after the nozzles were coated.

3.7 Determining PDE Configuration

Using a single spark-ignited thrust tube, tube length, spiral length, mixing length, sparking delay and firing frequency were varied to determine what conditions are most favorable for producing detonations. The combination of the optimized conditions would be the baseline engine setup used in the detonation branching experiments.

The thrust tube is designed to house the combustion process and the spiral is used to decrease DDT time. Due to weight considerations, the thrust tube and spiral should be the minimum lengths necessary to produce steady detonations. In this research, each thrust tube is 1.22 m with a 0.91 m spiral. The 1.22 m thrust tube extends 0.31 m beyond the spiral to allow the detonation to reach steady state before exiting the tube.

The mixing length must be long enough to ensure vaporization and homogeneous mixing, but short enough that the fuel does not cool and recondense. Increasing mixing length increased the PDE's efficiency by creating a completely vaporized and

homogeneous fuel-air mixture that lowered ignition and DDT times. The mixing length used in this research, as discussed in Section 3.3, is 4.9 m.

The PDE will not run repeatably on vaporized n-heptane with a cycle frequency less than 20 Hz. Also, the largest flow number attainable from the fuel nozzle stock is 3.6, which corresponds to a 20 Hz frequency, as calculated in Appendix A. A larger frequency would require more fuel and consequently a larger flow number, therefore the frequency is limited to 20 Hz.

Figure 3.20 shows cycle timelines for the two thrust tubes. At 20 Hz, the fill-detonation-exhaust cycle lasts 50 ms. The valving in the detonation-ignited thrust tube lags the valving in the spark-ignited thrust tube by one-quarter of a cycle, or 12.5 ms at 20 Hz.

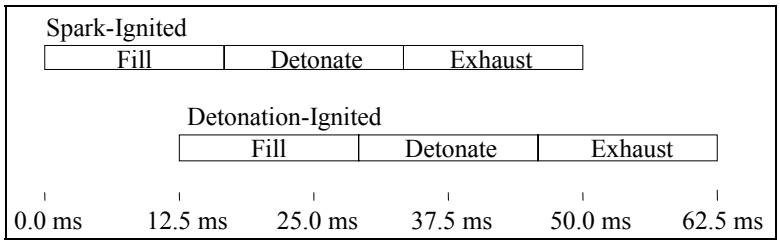

Fig. 3.20 Cycle timelines for both thrust tubes at 20 Hz

Sparking delay is the time from the moment the valves close at the end of the fill part of the cycle, signaling the beginning of the detonate part of the cycle, to the moment the three sparks have been deposited in the head of the spark-ignited thrust tube. Without a sparking delay, the spark would be introduced into the head of the spark-ignited thrust tube at the beginning of the detonate part of the cycle, indicated by the top arrow in Fig. 3.21. The detonation would form in the spark-ignited thrust tube, branch into the crossover tube and enter the head of the detonation-ignited thrust tube in the fill part of

the three-part cycle, indicated by the bottom arrow in Fig. 3.21. Introducing an ignition source during the fill part of the cycle causes a backfire.

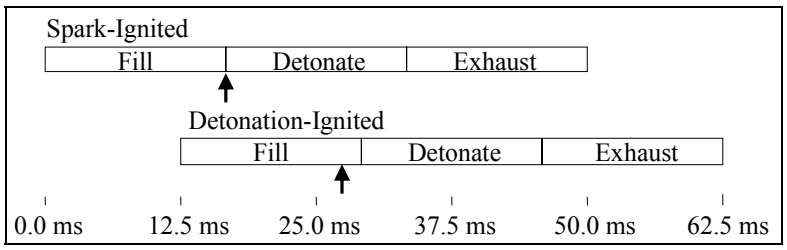

Fig. 3.21 Ignition sources deposited without a sparking delay

An 8 ms sparking delay inputs the spark into the head of the spark-ignited thrust tube 8 ms into the detonate part of the cycle, indicated by the top arrow in Fig. 3.22. The detonation would develop, branch into the crossover tube and enter the head of the detonion-ignited thrust tube, indicated by the bottom arrow in Fig. 3.22. Introducing an ignition source with an 8 ms sparking delay avoids a backfire.

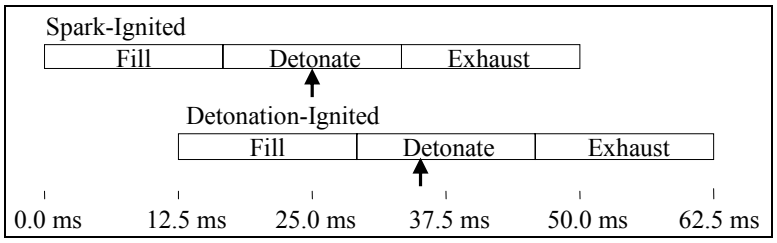

Fig. 3.22 Ignition sources deposited with an 8 ms sparking delay

Ignition performance improves with increased pressure. Figure 3.23 shows the head pressure without the ignition sources being introduced. In the detonate part of the cycle, the head pressure is above atmospheric after 7 ms and peaks between 9 and 12 ms. The 8 ms sparking delay allows the spark and the branched detonation to arrive in their respective thrust tube heads closer to the peak pressure than a 0 ms sparking delay would have.

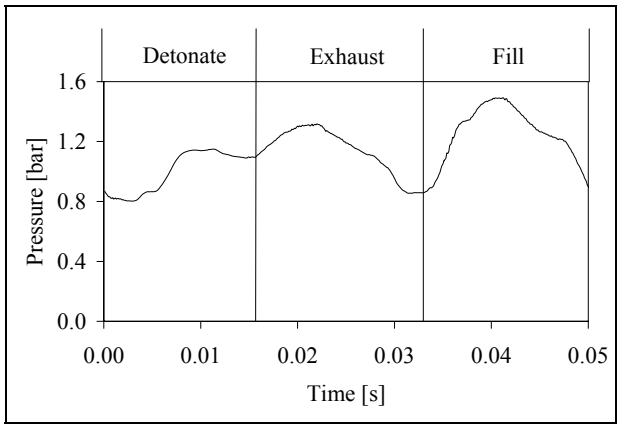

Fig. 3.23 Head pressure without combustion for one 20 Hz cycle

3.8 Velocities

The computer program for Calculation of Complex Chemical Equilibrium Compositions and Applications (CEA) developed by the NASA Lewis Research Center (Gordon and McBride, 1996) was used to calculate the theoretical C-J detonation velocity for heptane. Figure 3.24 shows the C-J detonation velocity for varying equivalence ratios.

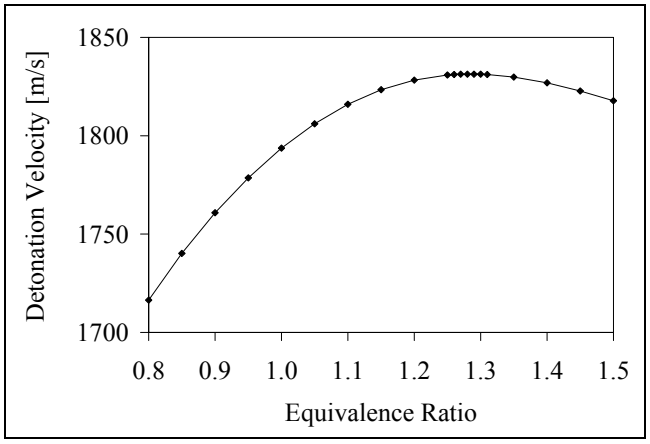

Fig. 3.24 N-heptane C-J detonation velocity versus equivalence ratio from CEA

Ion sensors provide data used in calculating combustion wave velocities. Each ion sensor registers a voltage drop as the combustion wave passes it and the voltage drop

and corresponding time are recorded by LabVIEW™ software. Dividing the distance between two ion sensors by the time it took the combustion wave to travel between them gives the wave velocity at the midpoint between the sensors.

3.9 Error Analysis

As with any experimental data, the results presented in this experiment have several sources of inherent error. First, there is error associated with measuring time. The data acquisition software was set to take 1,000,000 data points in 0.8 s, meaning one data point was taken every 0.8 μs, resulting in ±0.4 μs of error. While the software recorded many voltages at each data point, the voltages were not actually taken simultaneously, resulting in ±0.5 ns of error for each data point. The cumulative error for time measurements due to data acquisition limitations is ±0.4005 μs.

A source of time error that applies only to the pressure traces is the pressure transducers' reflected rise time of 1 μs. The ion sensor response time is less than the data acquisition time of 0.8 μs and is therefore a negligible error source.

The position measurements for the sensors are also error sources. Ion sensor and the pressure transducer positions were accurate to within ±1 mm. Also, the ion sensors have a 1.3 mm range in which the combustion wave can be detected, resulting in ±0.65 mm of error. The cumulative error for position measurements is ±1 mm for the pressure transducers and ±1.65 mm for the ion sensors.

Digitization also contributes to error. The data acquisition registered voltages in 2.442 mV steps, resulting in a ±1.221 mV error.

The pressure transducers used in this research have a resolution of 0.0036 bar and linearity less than or equal to 1% full scale, which equates to 3.4 bar. While more sensitive pressure transducers would have been preferable, pressure transducers with a large range were necessary to handle the detonations' von Neumann spikes. An OH sensor in the head of the spark-ignited thrust tube mirrored the pressure data from the pressure transducer in the head, shown in Fig. 3.25, proving the pressure transducers accurately show pressure rises due to ignition and detonation. In Fig. 3.25, the cycle lasts 50 ms and 0.00 s is the beginning of the detonate part of the cycle.

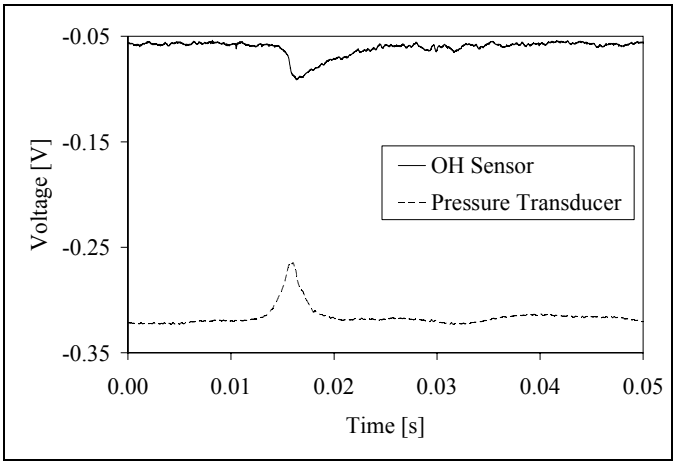

Fig. 3.25 Comparison of head OH sensor and pressure transducer readings

3.10 Chapter Summary

The vaporization system heats n-heptane pressurized at 40 bar to between 420 and 500 K and injects it into an airstream pressurized between 1.8 and 2.5 bar. As the fuel-air mixture flows through 4.9 m of mixing length, the heptane completely vaporizes and the fuel-air mixture becomes homogenous. The mixture flows into the manifold where it maintains a high enough temperature to prevent the fuel from recondensing. A dual

overhead cam system fills the thrust cylinder heads with the fuel-air mixture during the fill phase of the fill-detonate-exhaust cycle.

The PDE consists of one 1.22 m thrust tube with a 5.5 cm inner diameter, one 1.22 m thrust tube with a 5.6 cm inner diameter and one 1.22 m crossover tube with a 1.7 cm inner diameter. Each thrust tube has a 0.91 m Shelkin-like spiral to decrease DDT time. The first thrust tube spark-ignited. Part of the detonation from the spark-ignited thrust tube is branched into the crossover tube and the rest exits the thrust tube to produce thrust. The detonation in the crossover tube is deposited into the head of the second thrust tube to act as an ignition source. The entire detonation exits the tube to produce thrust.

Pressure transducers in the heads and ion sensors along the tubes take readings used in determining ignition and DDT times. Data was taken at a 20 Hz cycle frequency with an 8 ms sparking delay.

4 Results and Analysis

4.1 Introduction

This chapter describes the results of the detonation branching PDE research using liquid n-heptane. First, the effects of stoichiometry on the PDE performance are addressed to determine an appropriate equivalence ratio to use in testing. Then, to verify that detonations occur in both the spark- and detonation-ignited thrust tubes, the location of the detonation point in each tube is determined. The combustion wave speeds near the end of each thrust tube and the crossover tube are calculated and compared. Finally, ignition and DDT times are compared for the two thrust tubes to determine the time-savings from detonation ignition.

4.2 Stoichiometry

As the final step in determining the experimental setup, stoichiometry was tested to find the optimum equivalence ratio for the PDE. The C-J detonation velocity peaks at equivalence ratios between 1.27 and 1.30, as indicated in Fig. 3.24. However, the most fuel-efficient combustion occurs at stoichiometric conditions.

To determine the most fuel-efficient equivalence ratio that would repeatably produce combustion wave speeds on the order of detonation speeds, the PDE was run with equivalence ratios ranging from 0.90 to 1.40. It is important to note that the manifold geometry ensures the equivalence ratio is the same in both thrust tubes. Combustion wave velocities were calculated at each equivalence ratio in each thrust tube. Ion sensors were positioned 0.91 and 1.08 m from the head of the spark-ignited tube and 0.98 and 1.12 m from the head of the detonation-ignited tube, shown in Fig. 4.1.

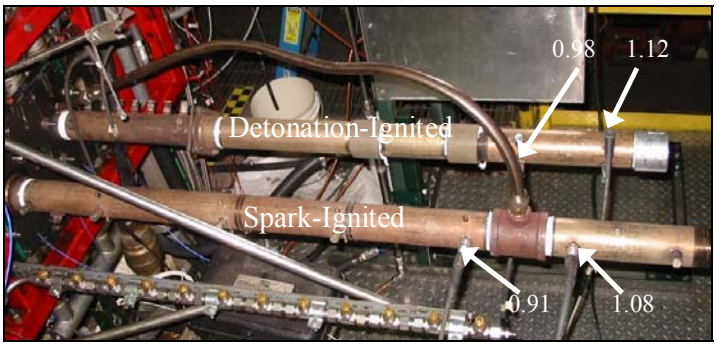

Fig. 4.1 Ion sensor locations in stoichiometry experiments in meters from the head

Each ion sensor registers a voltage drop as the combustion wave passes it, shown in Fig. 4.2. In the figure, 0.000 s indicates the beginning of the detonate part of the cycle in the spark-ignited thrust tube. The times when the combustion wave passes the ion sensors are used to calculate the combustion wave velocities at 1.00 m on the spark-ignited tube and 1.05 m on the detonation-ignited tube, the midpoints between the sensors. Table 4.1 shows the percentage of cycles that ignited and the average combustion wave velocity in each thrust tube for each equivalence ratio. Figure 4.3 shows the predicted C-J detonation velocity from Fig. 3.22 and the average combustion wave speeds from Table 4.1.

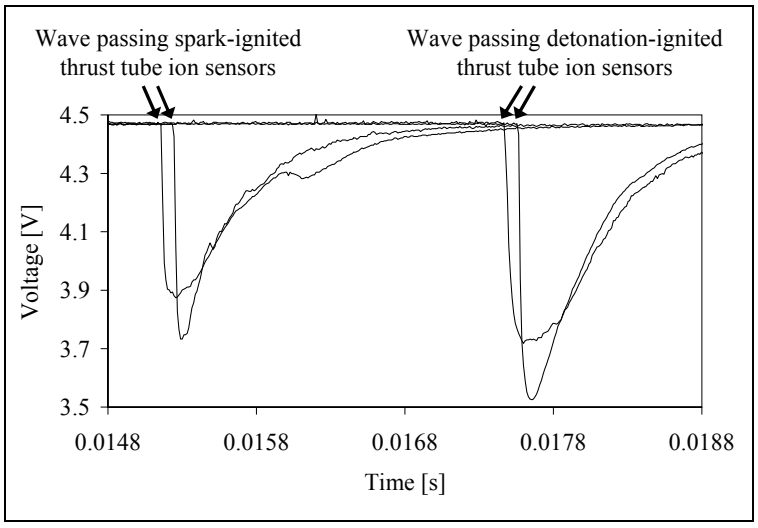

Fig. 4.2 Sample ion sensor voltage output in stoichiometry experiments

Table 4.1 Percent of cycles that ignited and average wave speeds

Equivalence Ratio	Spark-Ignited Thrust Tube		Detonation-Ignited Thrust Tube	
	% Ignited	Wave Speed [m/s]	% Ignited	Wave Speed [m/s]
0.90	100	2,008	88	1,334
0.97	100	2,376	100	1,539
1.00	100	2,089	100	1,456
1.02	100	2,180	100	1,592
1.20	100	1,877	27	1,660
1.40	100	1,754	0	N/A

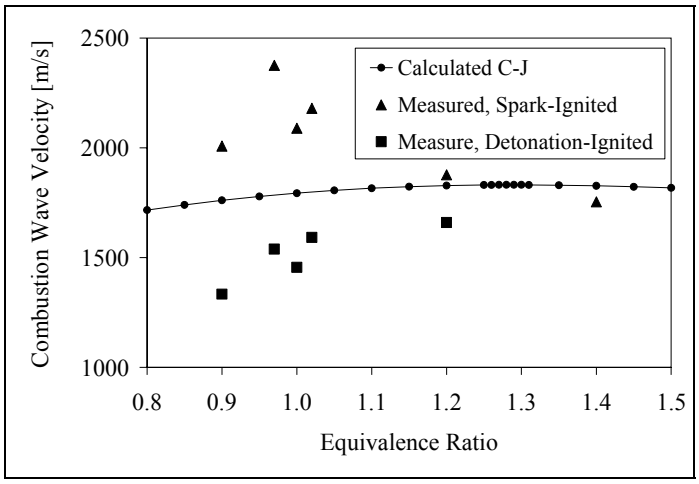

Fig. 4.3 CEA predicted C-J detonation velocity compared with measured wave speeds

Ideally, the PDE would follow the pattern set by the calculated C-J detonation wave speeds where the velocity peaks at fuel rich equivalence ratios between 1.27 and 1.30. However, measured combustion wave speeds in the spark-ignited thrust tube peak near an equivalence ratio of 1.00. Since the vaporization system was designed assuming stoichiometric conditions, there are vaporization and recondensing problems at fuel rich conditions that result in lower combustion wave speeds in the spark-ignited tube and fewer ignitions in the detonation-ignited tube.

This research concentrates on producing detonations in the detonation-ignited thrust tube. The experiments presented in the following sections take advantage of

repeatability in the detonation-ignited thrust tube at near-stoichiometric conditions and primarily use an equivalence ratio of 1.02.

4.3 Detonation Development

The first step in the detonation branching research is to locate the point where the combustion wave reaches detonation velocity. This provides information on how a detonation develops in the thrust tube and verifies that a branched detonation can be used as an ignition source. To determine the detonation point, one thrust tube was lined with ion sensors and the PDE was fired normally, with the first tube using spark ignition and the second tube using detonation ignition. The ion sensor readings were used to calculate combustion wave velocities.

Figure 4.4 shows ion sensors on the spark-ignited thrust tube. Figure 4.5 shows the ion sensor readings for 50 ms, one complete cycle at 20 Hz. In Fig. 4.5, the entire cycle lasts 0.05 s and 0.00 s indicates the beginning of the detonate part of the cycle in the spark-ignited thrust tube.

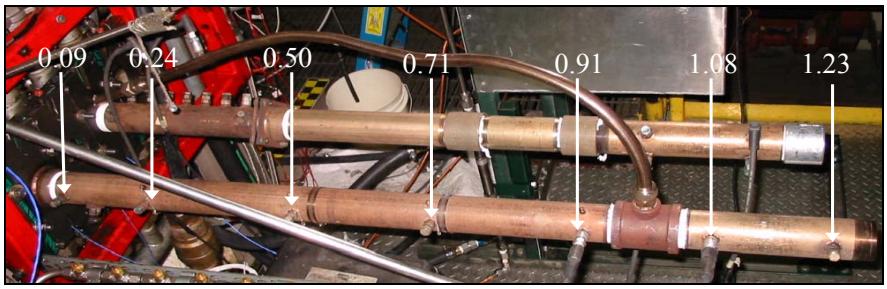

Fig. 4.4 Ion sensor positioning on spark-ignited thrust tube in meters from the head

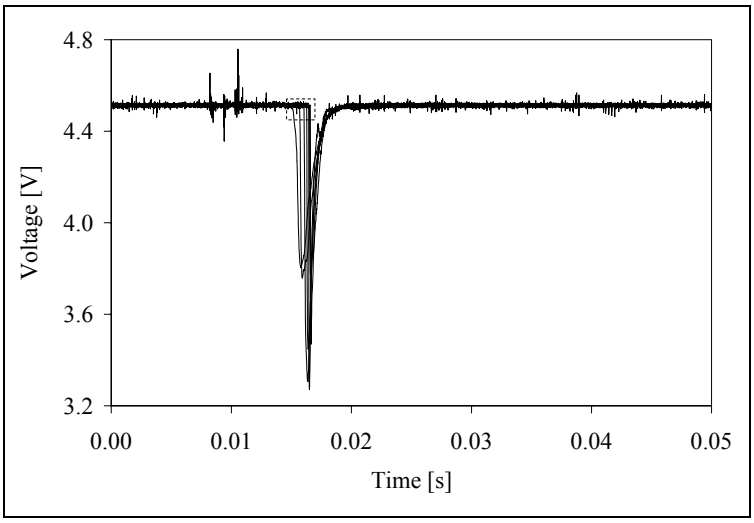

Fig. 4.5 Ion sensor readings for one cycle on the spark-ignited thrust tube

The area enclosed by the box in Fig. 4.5 is enlarged in Fig. 4.6 to show a detailed view of the voltage spikes recorded as the combustion wave crossed the ion sensors. In Fig. 4.6, ion sensor locations are indicated above the plot and the times when the combustion wave passed each sensor are on the x-axis; these distances and times are used to compute wave velocity. As the velocity increases and DDT occurs, the voltage drops become closer and steeper.

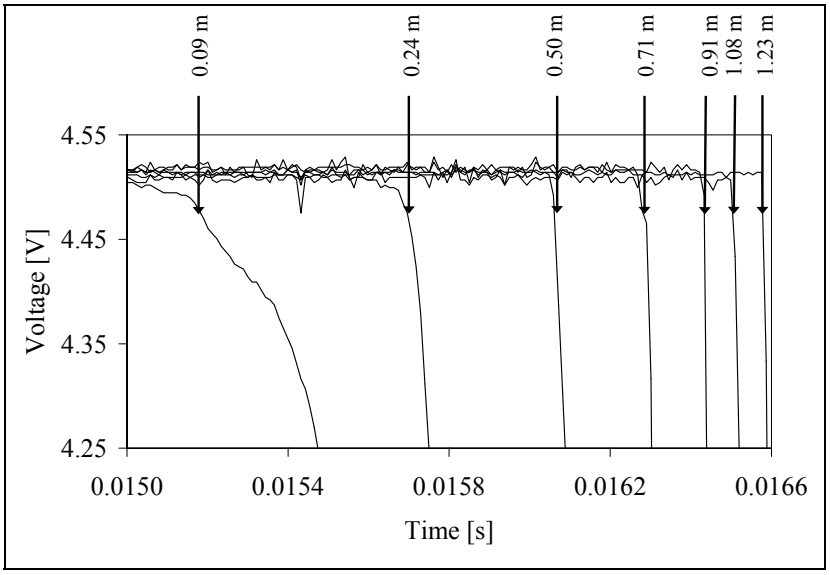

Fig. 4.6 Ion sensor location and readings for one cycle on the spark-ignited thrust tube

Readings from the ion sensors at 0.09, 0.24, 0.50, 0.71, 0.91, 1.08 and 1.23 m were used to calculate combustion wave velocities at 0.17, 0.37, 0.60, 0.81, 1.00 and 1.16 m, the midpoints between sensors. At a 20 Hz cycle frequency, data was taken for 0.8 s, capturing 16 cycles. Table 4.2 shows the wave speed at each velocity measuring point for each cycle.

Table 4.2 Wave speeds in m/s along spark-ignited thrust tube

Cycle	0.17 m	0.37 m	0.60 m	0.81 m	1.00 m	1.16 m
1	-2,721	605	939	1,346	2,013	1,954
2	558	917	1,213	1,175	2,707	1,905
3	186	430	1,155	1,058	2,580	1,905
4	381	483	1,366	1,392	2,064	1,905
5	163	540	1,234	1,155	2,707	1,954
6	309	568	1,661	1,401	2,393	1,954
7	493	587	939	972	2,393	2,032
8	314	506	1,542	1,539	2,172	1,929
9	353	526	1,186	958	2,013	1,954
10	163	397	1,048	1,075	2,798	1,979
11	187	1,257	2,570	1,346	2,064	1,905
12	-1,163	1,134	955	1,311	2,172	2,032
13	12,700	373	1,830	977	2,621	2,032
14	458	346	1,349	1,401	2,663	1,979
15	210	536	1,333	1,270	2,064	1,954
16	259	617	1,009	1,262	2,262	1,929

The velocity at 0.17 m is negative in cycles 1 and 12 because the ion sensors recorded the retonation wave at 0.09 and 0.24 m instead of the developing combustion wave. The velocity at 0.17 m for cycle 13 is three orders of magnitude larger than expected because the ion sensor at 0.09 m recorded the combustion wave and the sensor at 0.24 m recorded the retonation wave. Velocities at 0.17 m for cycles 1, 12 and 13 are not of the developing combustion wave because the ion sensors detected the retonation wave instead. Table 4.3 shows wave speeds at the 13 valid data points as well as the average wave speeds and standard deviations for the spark-ignited thrust tube.

Table 4.3 Valid wave speeds in m/s along spark-ignited thrust tube

Cycle	0.17 m	0.37 m	0.60 m	0.81 m	1.00 m	1.16 m
1	558	917	1,213	1,175	2,707	1,905
2	186	430	1,155	1,058	2,580	1,905
3	381	483	1,366	1,392	2,064	1,905
4	163	540	1,234	1,155	2,707	1,954
5	309	568	1,661	1,401	2,393	1,954
6	493	587	939	972	2,393	2,032
7	314	506	1,542	1,539	2,172	1,929
8	353	526	1,186	958	2,013	1,954
9	163	397	1,048	1,075	2,798	1,979
10	187	1,257	2,570	1,346	2,064	1,905
11	458	346	1,349	1,401	2,663	1,979
12	210	536	1,333	1,270	2,064	1,954
13	259	617	1,009	1,262	2,262	1,929
Average	310	593	1,354	1,231	2,375	1,945
± Error	4	4	13	13	37	31
Standard Deviation	132	242	418	182	289	38

Figure 4.7 shows the velocities from Table 4.2. The horizontal line in the plot indicates C-J detonation velocity at stoichiometric conditions, 1,794 m/s as indicated in Fig. 3.22. The thrust tube diagram at the top of Fig. 4.7 follows the x-axis scale; diagonal lines indicate the Shelkin-like spiral and marks on top of the tube indicate ion sensors.

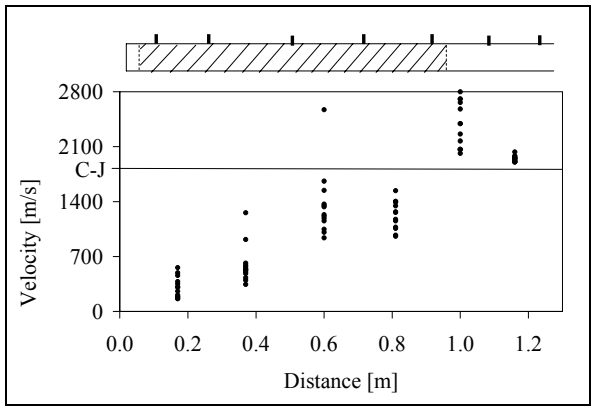

Fig. 4.7 Spark-ignited thrust tube and corresponding wave speeds

As seen in Fig. 4.7, the combustion wave speed tends to increase through the spiral. The peak at 1.0 m indicates a superdetonation wave. The combustion wave

reaches C-J detonation velocity between 0.81 and 1.00 m. The detonation point is the first point where the average wave speed is greater than or equal to the C-J detonation velocity. For the spark-ignited thrust tube, the detonation point is 1.00 m. It is important to note the close grouping of combustion wave velocities at 1.16 m, indicating small variation once the wave becomes a steady detonation.

The combustion wave velocity is expected to increase until it reaches C-J detonation velocity. The average velocity decreases slightly between 0.60 and 0.81 m, but the decrease is less than the range of calculated velocities at either location. The velocity also decreases between 1.00 and 1.16 m because the detonation wave speed decreases to C-J detonation velocity after spiking with the superdetonation wave.

The detonation point was also determined for the detonation-ignited thrust tube. Figure 4.8 shows the ion sensor placement on the detonation-ignited thrust tube. Since the thrust tubes were made from already existing parts rather than machined specifically for this experiment, ion sensors were not at the same locations on both tubes. Readings from the ion sensors at 0.08, 0.19, 0.30, 0.43, 0.58, 0.75 and 0.90 m were used to calculate average combustion wave velocities at 0.13, 0.25, 0.37, 0.51, 0.67 and 0.83 m, the midpoints between the sensors.

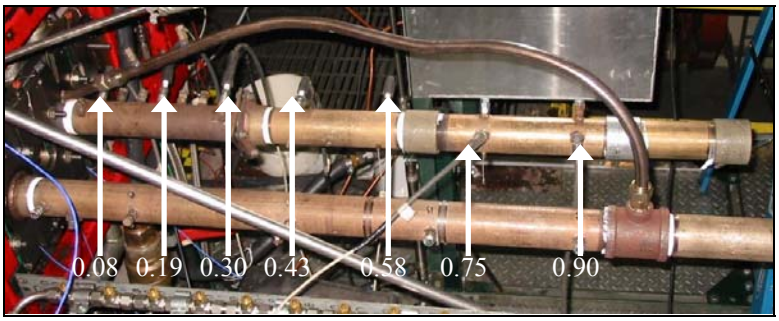

Fig. 4.8 Ion sensors on detonation-ignited thrust tube in meters from the head

The cycle frequency was 20 Hz and data was taken for 0.8 s, capturing 16 cycles. Table 4.4 shows the wave speeds. Figure 4.9 shows the velocities from Table 4.4 with the corresponding thrust tube diagram above the plot.

Table 4.4 Wave speeds in m/s along detonation-ignited thrust tube

Cycle	0.13 m	0.25 m	0.37 m	0.51 m	0.67 m	0.83 m
1	378	328	638	729	2,038	2,005
2	391	438	510	1,191	1,065	2,381
3	294	361	458	1,385	2,231	1,954
4	396	398	396	1,524	1,310	1,859
5	417	382	559	1,073	1,423	1,905
6	482	339	410	1,181	1,775	2,117
7	401	369	396	1,044	1,603	1,905
8	386	302	1,649	798	1,423	1,814
9	457	298	765	1,044	1,448	1,836
10	428	332	527	751	2,201	2,005
11	441	371	416	2,209	1,300	1,814
12	345	350	683	1,030	1,423	1,881
13	345	411	428	1,066	1,619	2,005
14	394	513	364	1,509	1,529	1,836
15	423	329	672	782	2,428	1,793
16	486	302	429	1,604	1,720	1,929
Average	404	364	581	1,182	1,659	1,940
± Error	6	6	8	16	23	30
Standard Deviation	49	55	300	378	372	143

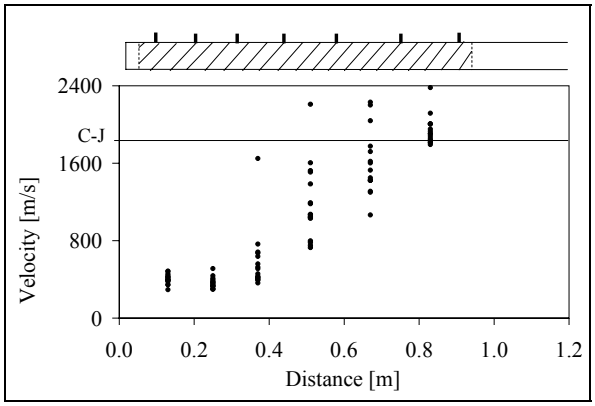

Fig. 4.9 Detonation-ignited thrust tube and corresponding wave speeds

As seen in Fig. 4.9, the wave speeds tend to increase through the spiral. The detonation point, the first point where the calculated combustion wave speed is greater than or equal to C-J detonation velocity, is at 0.83 m for the detonation-ignited thrust tube, approximately 0.17 m ahead of the detonation point in the spark-ignited tube.

The average combustion wave velocities at 0.17 and 0.25 m did not follow the expected trend of increasing velocity. However, this is in the initial stages of DDT and the difference between the velocities is smaller than the data range at either location.

4.4 Measured Events

This section discusses the instrumentation used to determine wave speeds and ignition and DDT times in Sections 4.5, 4.6 and 4.7. The PDE was instrumented with a pressure transducer each thrust tube head and a pair of ion sensors along the thrust and crossover tubes. A spark trace was also recorded.

Figure 4.10 shows the ion sensors. In the spark-ignited tube, ion sensors were 0.91 and 1.08 m from the head. In the crossover tube, they were 0.20 and 0.30 m from the detonation-ignited thrust tube head. In the detonation-ignited thrust tube, they were 0.98 and 1.12 m from the head.

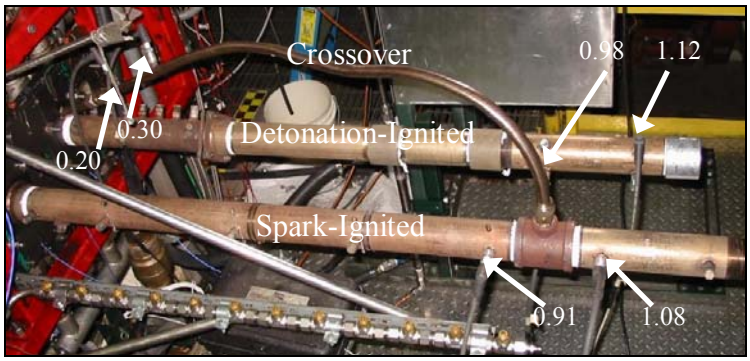

Fig. 4.10 PDE ion sensors in meters from the head

Using voltage changes, LabVIEW™ recorded pressure traces in each thrust tube head and the combustion wave passing the ion sensors. Figure 4.11 shows a sample output of one cycle where the step on the left is the spark trace, the six downward spikes are the ion sensor traces and the two voltage increases are the head pressure transducer traces. In Fig. 4.11, the entire cycle is 0.05 s and 0.00 s is the beginning of the detonate part of the cycle in the spark-ignited thrust tube. The dashed box in Fig. 4.11 was enlarged in Fig. 4.12.

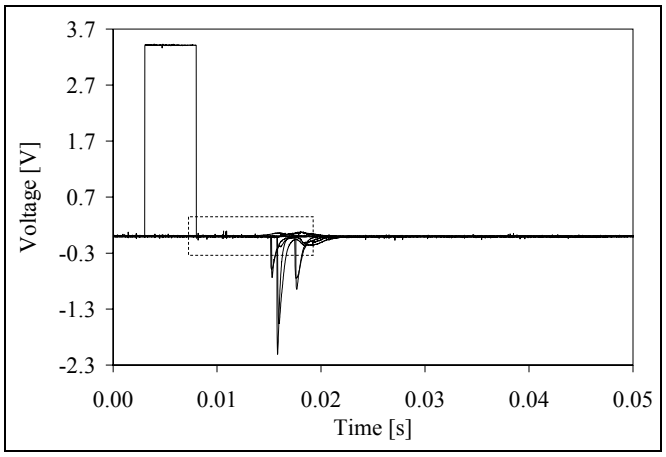

Fig. 4.11 Ion sensor and pressure transducer readings for one cycle

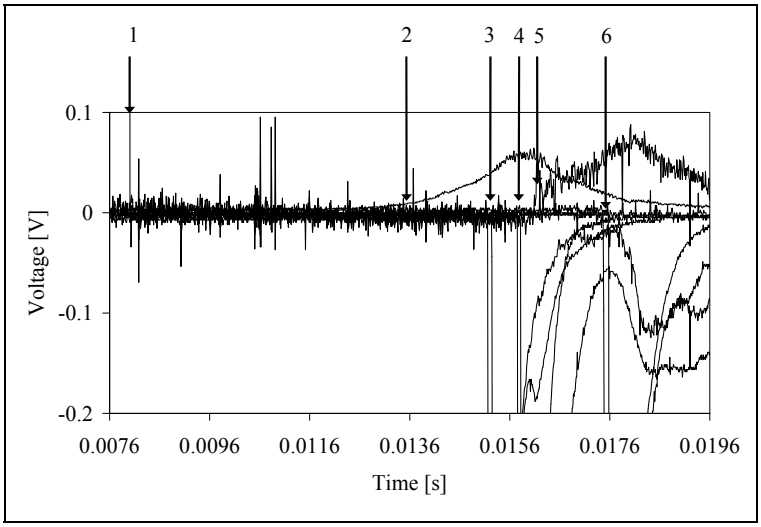

Fig. 4.12 Enlargement of Fig. 4.11

In Fig. 4.12, 1 is the sparking completion at the 8 ms sparking delay. At 2, the pressure transducer in the spark-ignited thrust tube head shows the pressure rise indicating ignition. The downward spikes at 3 and 4 indicate the detonation wave passing the ion sensors in the spark-ignited and crossover tubes, respectively. At 5, the pressure transducer in the detonation-ignited thrust tube head shows the pressure rise indicating ignition. The downward spikes at 6 indicate the detonation wave passing the detonation-ignited tube's ion sensors. These events will be discussed in detail in the next sections.

4.5 Wave Speeds

Figure 4.10 shows the ion sensor locations for the wave speed experiments. To ensure a detonation was branched from the spark-ignited thrust tube, the wave speed was measured in the thrust tube where the crossover tube connects. To ensure a detonation arrived in the detonation-ignited tube, the wave speed was measured in the crossover tube just downstream of the detonation-ignited tube head. The wave speed was also measured near the open end of the detonation-ignited tube.

In the spark-ignited tube, ion sensors 0.91 and 1.08 m from the head gave the velocity at 1.00 m. In the crossover tube, sensors at 0.20 and 0.30 m from the head of the detonation-ignited tube head gave the velocity at 0.25 m. In the detonation-ignited thrust tube, sensors at 0.98 and 1.12 m from the head gave the velocity at 1.05 m. A voltage drop registered as the combustion wave passed each ion sensor, shown in Fig. 4.12. Dividing the distance between the ion sensors by the time it took the voltage wave to traverse them yields the combustion wave velocity.

The cycle frequency was 20 Hz and data was taken for 0.8 s, resulting in 16 velocity measurements at each location. Table 4.5 shows the cycle velocities in each tube as well as their averages and standard deviations.

Table 4.5 Combustion wave velocities near the end of each tube

Cycle	Spark-Ignited Thrust Tube [m/s]	Crossover Tube [m/s]	Detonation-Ignited Thrust Tube [m/s]
1	2,201	1,639	1,623
2	2,262	1,588	1,587
3	2,359	1,782	1,587
4	2,117	1,613	1,587
5	2,325	1,588	1,521
6	1,795	1,639	1,605
7	2,293	1,588	1,679
8	2,231	1,639	1,587
9	2,262	1,666	1,623
10	2,540	1,613	1,554
11	2,144	1,666	1,660
12	1,738	1,539	1,521
13	1,795	1,563	1,660
14	2,201	1,666	1,490
15	2,325	1,613	1,605
16	2,293	1,752	1,587
Average	2,180	1,634	1,592
± Error	33	22	22
Standard Deviation	216	62	50

The velocity in the spark-ignited thrust tube was calculated at the detonation point, as determined in Section 4.3. Due to the superdetonation wave, the average wave speed was 2,180 m/s, well above the C-J detonation velocity of 1,794 m/s for an equivalence ratio of 1.02. This indicates that a strong detonation is branched into the crossover tube. Figure 4.13 shows the spark-ignited thrust tube's wave velocities at the branching point for each cycle as well as the average velocity, indicated by the dashed horizontal line, and the C-J detonation velocity, indicated by the solid horizontal line.

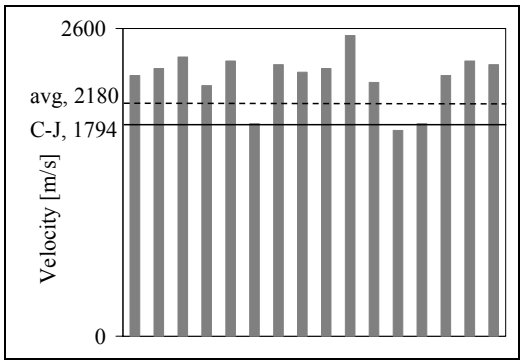

Fig. 4.13 Spark-ignited thrust tube combustion wave speeds at crossover

In the crossover tube, the average wave speed near the exit into the second thrust tube was 1,634 m/s. While the average combustion wave in the crossover tube has a velocity 9% below C-J detonation velocity, its velocity is on the order of a detonation, which has a velocity on the order of km/s. Therefore, the combustion wave in the crossover tube had a pressure and density increase across the flame slightly less than a C-J detonation wave, but on the same order of magnitude, which is an order of magnitude above that of a deflagration. Figure 4.14 shows the crossover tube's wave velocities for each cycle as well as the average velocity and the C-J detonation velocity.

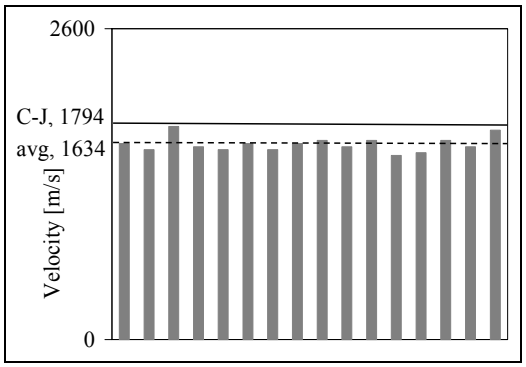

Fig. 4.14 Crossover tube combustion wave speeds near detonation-ignited tube head

The velocity in the detonation-ignited thrust tube was calculated 1.05 m from the head, 0.22 m beyond the detonation point of 0.83 m determined in Section 4.3. At 1.05 m, the average wave speed was 1,592 m/s, which is the same order of magnitude as the

C-J detonation velocity, but 11% lower. This is because the wave speed peaked closer to the head and had already slowed beyond C-J detonation velocity by 1.05 m. Also, the fuel-air mixture at the end of the tube is lean, contributing to the velocity decrease at the tube end. Figure 4.15 shows the detonation-ignited tube's wave velocities for each cycle as well as the average and C-J detonation velocities.

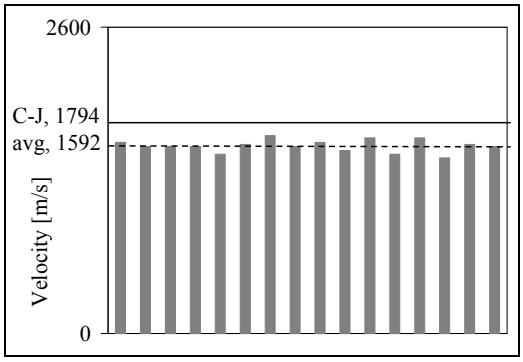

Fig. 4.15 Detonation-ignited thrust tube combustion wave speeds near the tube end

Figure 4.16 compares the average head pressures in the thrust tubes. In the figure, the entire cycle is 0.000 s indicates the beginning of the detonate part of the cycle in the spark-ignited thrust tube. The detonation-ignited thrust tube has a 33% stronger pressure spike than the spark-ignited thrust tube, indicating a stronger detonation. The exit velocity in the detonation-ignited tube is lower because the combustion wave in that tube developed into a detonation in less distance than in the spark-ignited tube, as discussed in Section 4.3, and therefore began slowing down earlier.

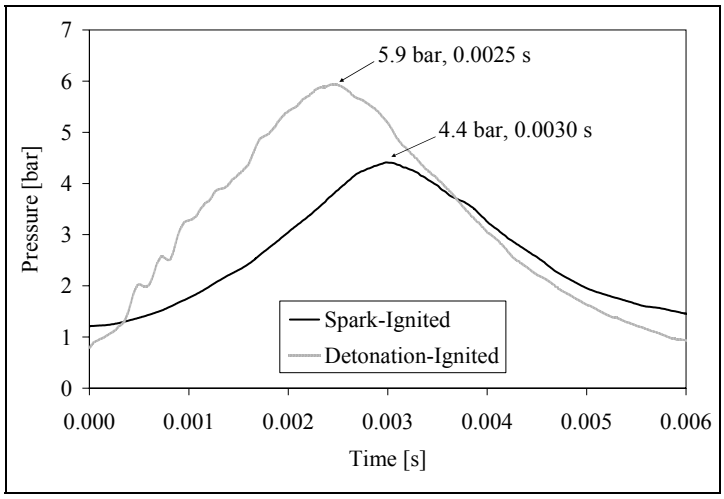

Fig. 4.16 Head pressure traces for both tubes

In summary, a strong detonation was branched from the spark-ignited thrust tube to the crossover tube. A combustion wave with a velocity slightly less than, but on the order of the C-J detonation velocity was branched from the crossover tube to the detonation-ignited thrust tube head. The detonation in the detonation-ignited tube was stronger than in the spark-ignited thrust tube, but the wave speed in the detonation-ignited thrust tube was measured after it slowed below C-J detonation velocity.

4.6 Ignition Time Savings

In the spark-ignited thrust tube, ignition delay is the time from the spark being deposited in the head until the pressure transducer in the head indicates a pressure rise associated with combustion. Due to the sparking delay, sparks were deposited in the head 8 ms into the detonate part of the cycle. Ignition occurs when the head pressure trace slope can be differentiated from the noise in the system; in this case, ignition occurred when the voltage trace from the head pressure transducer was 2.5 V/s for 0.5 ms.

The pressure transducer in the spark-ignited thrust tube head was calibrated to 1 V = 73.90 bar. Figure 4.17 shows the pressure trace for the spark-ignited head, indicating when the spark was input in the head and when combustion occurred. In the figure, 0.0000 s is the beginning of the detonate part of the cycle in the spark-ignited thrust tube.

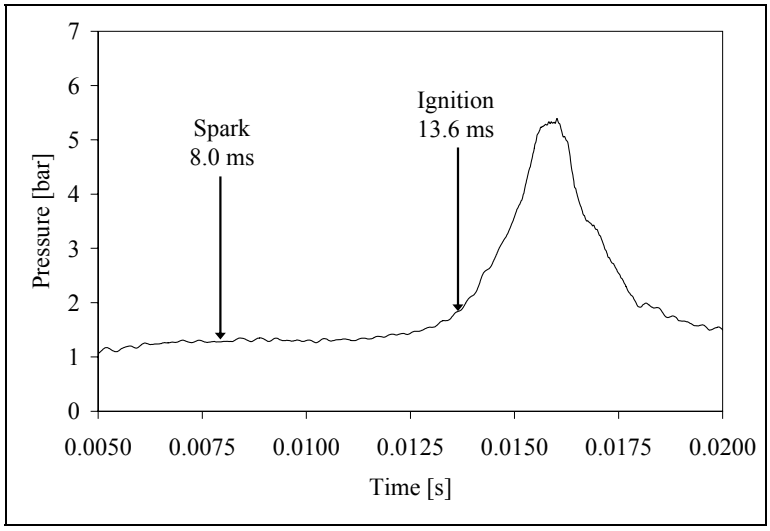

Fig. 4.17 Spark-ignited tube head pressure trace

At a 20 Hz cycle frequency, data was taken for 0.8 s, resulting in 16 data points. Table 4.6 shows the ignition delay at each data point as well as the average ignition delay and the standard deviation. The average ignition delay, the time between the spark and ignition, is 5.6 ms.

Table 4.6 Ignition delay in spark-ignited thrust tube

Cycle	Ignition Delay [ms]
1	5.882
2	4.747
3	5.057
4	5.991
5	5.563
6	5.467
7	5.488
8	5.547
9	5.288
10	6.566
11	5.951
12	5.439
13	6.154
14	5.632
15	5.415
16	5.919
Average	5.632
± Error	0.004
Standard Deviation	0.439

The pressure transducer in the detonation-ignited thrust tube was calibrated to 1 V = 72.65 bar. Figure 4.18 shows the detonation-ignited thrust tube head pressure with 0.0125 s indicating the beginning of the detonate part of the cycle in that tube. The sharp pressure rise at 17.0 ms is the shock wave from the detonation entering the head. The detonation creates a pressure and temperature rise that allow almost immediate ignition. Ignition delay is the time between the shock arriving in the head and the pressure rise following the shock. Table 4.7 shows the ignition delay for each cycle as well as the average ignition delay and standard deviation.

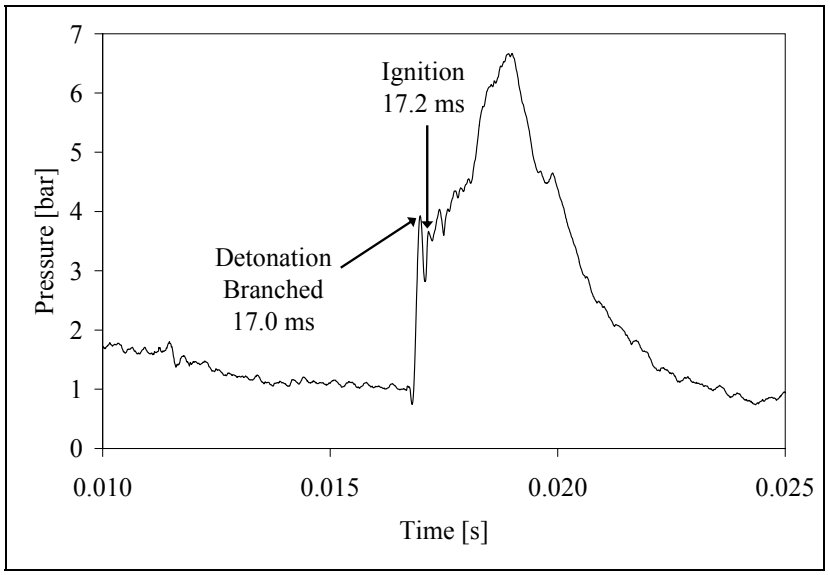

Fig. 4.18 Detonation-ignited tube head pressure trace

Table 4.7 Ignition delay in detonation-ignited thrust tube

Cycle	Ignition Delay [ms]
1	0.187
2	0.187
3	0.187
4	0.198
5	0.165
6	0.187
7	0.187
8	0.198
9	0.187
10	0.209
11	0.187
12	0.209
13	0.187
14	0.187
15	0.187
16	0.176
Average	0.189
± Error	0.004
Standard Deviation	0.011

Detonation branching reduced average ignition delay from 5.63 to 0.19 ms, a 5.44 ms time-savings in the ignition portion of the detonate part of the cycle.

4.7 Deflagration to Detonation Transition Time Savings

DDT time is the time between ignition and the combustion wave passing the detonation point. For the spark-ignited tube, an ion sensor at 0.91 m approximated the detonation point, a reasonable location based on the 1.00 m indicated in Fig. 4.7. For the detonation-ignited tube, the ion sensor was at 0.98 m, 0.15 m beyond the detonation point according to Fig. 4.9. To account for the 0.15 m between the detonation point and the ion sensor, 80 μs, the time it takes a C-J detonation wave to travel 0.15 m, was subtracted from the voltage spike time to calculate DDT times.

Figure 4.19 shows the spark-ignited thrust tube ignition point, indicated on the head pressure trace, and the voltage drop from the combustion wave passing the 0.91 m ion sensor. In the figure, 0.000 s is the beginning of the detonate part of the cycle in the spark-ignited thrust tube. DDT time is the time between ignition and the voltage drop.

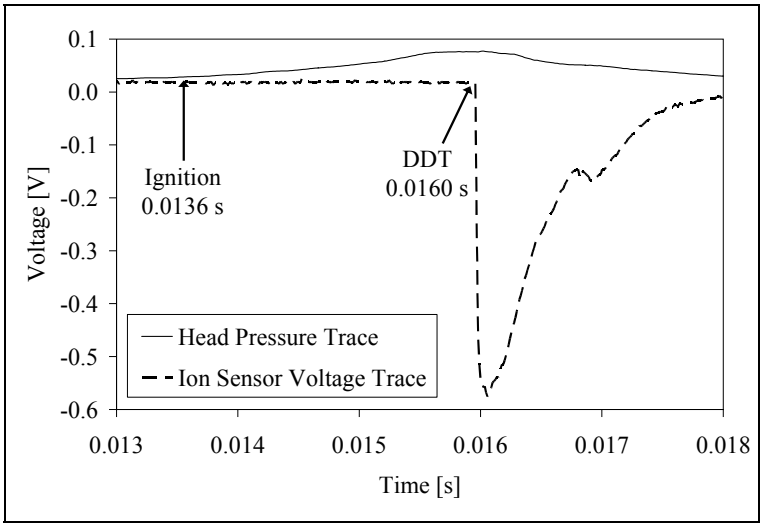

Fig. 4.19 Head pressure and ion sensor voltage traces showing ignition and DDT points for the spark-ignited thrust tube

Figure 4.20 shows the detonation-ignited thrust tube ignition point, indicated on the head pressure trace, and the voltage drop from the combustion wave passing the 0.98

m ion sensor. In the figure, 0.000 s is the beginning of the detonate part of the cycle in the spark-ignited thrust tube. DDT time is the time between ignition and the voltage drop minus 80 μs.

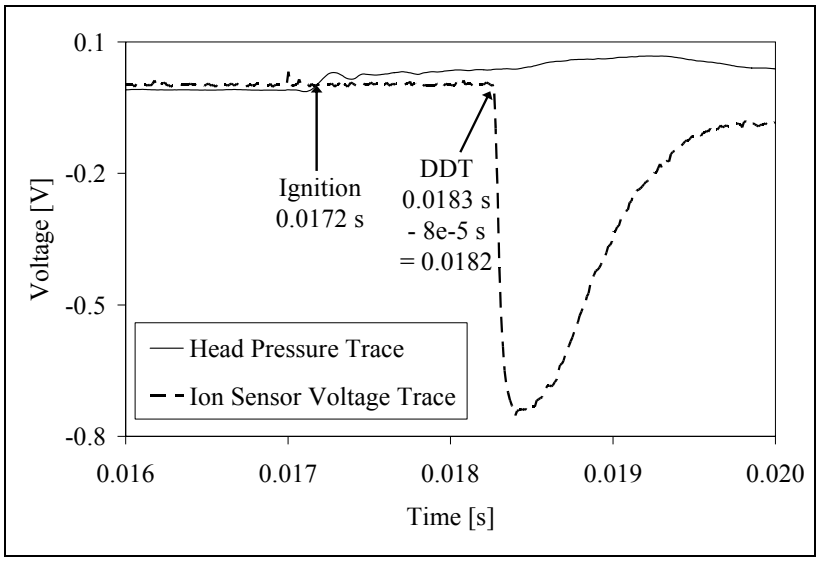

Fig. 4.20 Head pressure and ion sensor voltage traces showing ignition and DDT points for the detonation-ignited thrust tube

Table 4.8 gives DDT times for both thrust tubes for 16 50 ms cycles as well as average DDT times and standard deviations. Average DDT time for the detonation-ignited thrust tube was 44% of the spark-ignited tube DDT time, showing time-savings from using a detonation ignition source.

Table 4.8 DDT times for each thrust tube

Cycle	Spark-Ignited Thrust Tube [ms]	Detonation-Ignited Thrust Tube [ms]
1	2.333	1.064
2	2.418	0.998
3	2.383	0.943
4	2.410	1.163
5	2.422	1.141
6	2.479	0.921
7	2.272	1.009
8	2.190	1.097
9	2.263	1.064
10	2.776	1.042
11	2.307	1.053
12	2.322	0.998
13	2.415	0.954
14	2.242	1.108
15	2.254	0.932
16	2.337	1.009
Average	2.364	1.031
± Error	0.001	0.001
Standard Deviation	0.136	0.074

4.8 Chapter Summary

Detonation-branching experiments used a near-stoichiometric equivalence ratio of 1.02. The experiments prove that not only is detonation ignition feasible, but it results in appreciable cycle time savings over spark ignition. Ignition times are 5.63 and 0.19 ms for the spark- and detonation-ignited thrust tubes, respectively. DDT times are 2.36 and 1.03 ms for the spark- and detonation-ignited thrust tubes, respectively. The total time savings in the detonate part of the PDE cycle for detonation-ignition is 6.77 ms, an 85% time reduction in detonation development, as shown in Fig. 4.21.

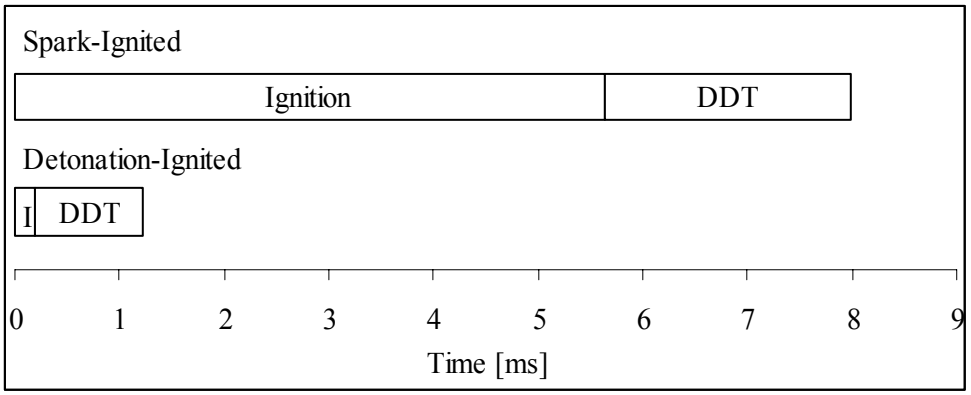

Fig. 4.21 Average ignition and DDT times for each thrust tube

Also, DDT is complete in 0.83 m in the detonation-ignited thrust tube, compared with 1.00 m in spark-ignition, which allows for a shorter tube, resulting in weight savings.

5 Recommendations and Conclusions

5.1 Conclusions

The testing proves that branched detonations can be successfully used as ignition sources with liquid hydrocarbon fuels. A vaporization system vaporized liquid n-heptane and ensures a homogenous fuel-air mixture. Temperatures were monitored throughout the system to ensure conditions did not allow the fuel to recondense. The PDE in these experiments had two 1.22 m thrust tubes, each with a 0.91 m Shelkin-like spiral. One thrust tube was spark-ignited and the other was detonation-ignited via a 1.22 m crossover tube from the spark-ignited thrust tube. The cycle frequency was 20 Hz and the sparking delay was 8 ms.

The branched detonation had more energy than the spark, allowing ignition and DDT to occur in less distance and time. Operating at 20 Hz and a 1.02 equivalence ratio, DDT occurred in 1.00 m in the spark-ignited thrust tube and 0.83 m in the detonation-ignited tube, meaning the detonation-ignited thrust tube formed a detonation in 83% of the length that the spark-ignited thrust tube did. A PDE using primarily detonation-ignited thrust tubes as opposed to spark-ignited thrust tubes could reduce tube length by 17% for an appreciable weight savings. Also, the spiral length could be reduce to decrease drag and increase thrust.

Ignition times were 5.63 and 0.19 ms and DDT times were 2.36 and 1.03 ms for the spark- and detonation-ignited thrust tubes, respectively. The total time savings in the detonate part of the PDE cycle for detonation-ignition was 6.77 ms, an 85% time reduction in ignition and DDT times. One way to capitalize on the decreased ignition and DDT time is to reduce overall cycle length, affording an appreciable thrust increase.

Another way is to increase the fill part of the cycle by the amount of time the detonate part decreased. This would keep the overall cycle length constant, but lessen the pressure requirements to fill the tube with the combustible mixture.

5.2 Recommendations

This research was a proof of concept, as opposed to a design optimization. Future research should include design optimization studies as well as proof of concept research that build on the concepts proven in this research.

Several aspects of the vaporization system should be optimized for use in flight. First, the vaporization process should be optimized by increasing the furnace temperature to 540 K so the fuel is vaporized upon injection into the airstream, allowing mixing length reduction. The mixing process between vaporized fuel and the airstream should be studied to provide a better understanding of how to obtain a homogeneous mixture. Also, the feasibility of drawing heat from the thrust and crossover tubes to heat the fuel should be examined. This would eliminate the need for a furnace and would cool the thrust and crossover tubes, potentially extending tube life.

Second, the PDE should be optimized to produce maximum thrust. The effects of thrust tube length and diameter, spiral shape and position, firing frequency, stoichiometry and detonation branching on thrust should be determined.

Third, a proof of concept study should be done to focus a branched detonation in the head to increase the amount of energy available for DDT, thereby eliminating the need for a spiral or similar DDT enhancing device. Since DDT enhancing devices cause drag in the thrust tubes, removing them would increase the PDE's thrust.

Fourth, a proof of concept study should examine the feasibility of a self sustaining PDE. To do this, a series of parallel thrust tubes would be arranged in a circle and connected by crossover tubes. One thrust tube would be ignited one time with a spark and from then on detonation branching would be the ignition source, making the PDE self-igniting.

Appendix A. Flow Number Calculation

Given

Stoichiometric fuel to air ratio on a mass basis

$FA \equiv 0.065988$

Injected air temperature [R]

$Tair \equiv 560$

Universal gas constants for air and heptane [ft lbf / lbm R]

$Rair \equiv 53.34$

$Rfuel \equiv 15.42$

Volume fuel-air mixture must fill [ft^3]

$Vfill := \frac{378.9}{12^3}$ $\quad Vfill = 0.219$

Pressure in head and tubes (atmospheric pressure) [lbf / ft^2]

$patm \equiv 2116.2$

Calibration density for heptane [lbm / ft^3]

$\rho cal \equiv 47.75$

Firing frequency [Hz]

$freq \equiv 20$

Fuel temperature [R]

$Tfuel \equiv 760$

Furnace volume [ft^3]

$Vfurnace \equiv .03954$

Furnace pressure [psi]

$pfurn \equiv 600$

Find

Fuel-air mixture temperature [R]

$Tavg := 1$

Fuel and air mass flow rates [lbm / s]

$mdotfuel := 1$

$mdotair := 1$

Fuel and air volumetric flow rates [ft^3 / s]

$Vdotfuel := 1$

$Vdotair := 1$

Given

$$Tavg = \frac{mdotfuel \cdot Tfuel + mdotair \cdot Tair}{mdotfuel + mdotair}$$

$$\frac{mdotfuel}{mdotair} = FA$$

$$Vdotair = \frac{mdotair \cdot Rair \cdot Tavg}{patm}$$

$$Vdotfuel = \frac{mdotfuel \cdot Rfuel \cdot Tavg}{patm}$$

$$Vdotfuel + Vdotair = Vfill \cdot freq$$

Result := Find(Tavg, mdotfuel, mdotair, Vdotfuel, Vdotair)

$Tavg := Result_0$ $\quad Tavg = 572.381$

$mdotfuel := Result_1$ $\quad mdotfuel = 0.02$

$mdotair := Result_2$ $\quad mdotair = 0.298$

$Vdotfuel := Result_3$ $\quad Vdotfuel = 0.082$

$Vdotair := Result_4$ $\quad Vdotair = 4.303$

Find fuel density [lbm/ft^3] for fuel in furnace using SUPERTRAPP

at 600 psi in furnace, SUPERTRAPP gives density

$$\rho furnhi := 3.1843918717 \cdot 10^{-14} \cdot Tfuel^6 - 1.5279974578 \cdot 10^{-10} \cdot Tfuel^5 \ldots + 3.0134533346 \cdot 10^{-7} \cdot Tfuel^4 - 3.1281117940 \cdot 10^{-4} \cdot Tfuel^3 \ldots + 1.8030805190 \cdot 10^{-1} \cdot Tfuel^2 - 5.4759931153 \cdot 10 \cdot Tfuel + 6.8945210049 \cdot 10^3$$

$\rho furnhi = 35.222$

Find fuel nozzle flow number; mdotfuel [lbm/hr], p [psig], ρ [lbm/ft^3]

at 600 psi in furnace

$$FNhi := \frac{mdotfuel \cdot 60^2}{\sqrt{pfurn - 2 \cdot \frac{patm}{144}}} \cdot \sqrt{\frac{\rho cal}{\rho furnhi}}$$

$\boxed{FNhi = 3.454}$

Find run time [min] using this fuel temperature and flow rate

at 600 psi in furnace

$$thi := \frac{\rho furnhi \cdot Vfurnace}{mdotfuel \cdot 60}$$

$\boxed{thi = 1.179}$

Bibliography

Brophy, C., D. Sinibaldi, D. Netzer and R. Johnson. "Operation of a JP-10/Air Pulse Detonation Engine," AIAA 2000-3591, 36th Joint Propulsion Conference, July 2000, Huntsville AL.

Darrah, S. "Jet Fuel Deoxygenation," AF Wright Aeronautical Laboratories Interim Report for March 1987 - July 1988.

Doungthip, Thammarat, Jamie S. Ervin, Theodore F. Williams, and Jarrod Bento, "Studies of Injection of Jet Fuel at Supercritical Conditions," *Industrial & Engineering Chemistry Research*, Vol. 41, No. 23, 2002.

Ervin, J. S., T. F. Williams, and G. Hartman, "Effect of Test Period on the Rate of Fouling in a Complex Flowing System," Structure of Jet Fuels V. Boston MA, August 1998.

Flathead Valley Community College (FVCC), http://mail.fvcc.edu/~pmartino/gc.tcd.inf.html. 21 February 2004.

Glassman, Irvin. *Combustion*. New York: Academic Press, 1996.

Gordon, S and McBride B. "Computer Program for Calculation of Complex Chemical Equilibrium Compositions and Applications", NASA RP 1311 I&II, October 1994 and June 1996.

Heneghan, S. P., C. R. Martel, T. F. Williams and D. R. Ballal, "Effects of Oxygen and Additives on the Thermal Stability of Jet Fuels," University of Dayton; Dayton OH, undated.

Huber, M. L. "NIST Thermophysical Properties of Hydrocarbon Mixtures Database (SUPERTRAPP) Version 3.1 Users' Guide," U.S. Department of Commerce, Feb 2003.

Kanury, Marty A. *Introduction to Combustion Phenomena*. New York: Gordon and Breach, 1975.

Kuo, Kenneth K. *Principles of Combustion*. New York: John Wiley & Sons, Inc., 1986.

Lewis, Bernard and Guenther von Elbe. *Combustion, Flames and Explosions of Gases*. New York: Academic Press Inc., 1961.

National Institutes of Standards and Technology (NIST) Standard Reference Database Number 69 (NIST, 2003) March, 2003 Release, http://webbook.nist.gov/chemistry.

Restek Corporation, 2003.

Rolling, August J. *Alternative Pulse Detonation Engine Ignition System Investigation through Detonation Splitting*. MS thesis, AFIT/GAE/ENY/02-10. Graduate School of Engineering and Management, Air Force Institute of Technology (AU), Wright-Patterson AFB OH, March 2002 (ADA40512).

Rolling, August J., Paul I. King and Fred R. Schauer. "Propagation of Detonation Waves in Tubes Split from a PDE Thrust Tube," AIAA 2002-3714, 38th AIAA/ASME/SAE/ASEE Joint Propulsion Conference and Exhibit, 7-10 July 2002, Indianapolis IN.

Schauer, Fred, Jeff Stutrud, and Royce Bradley. "Detonation Initiation Studies and Performance Results for Pulsed Detonation engine Applications," AIAA 2001-1129, 39th AIAA Aerospace Sciences Meeting & Exhibit, 8-11 January 2001, Reno NV.

Schultz, E., E. Wintenberger and J. Shepherd. "Investigation of Deflagration to Detonation Transition for Application to Pulse Detonation Engine Ignition Systems." Proceedings of the 16th JANNAF Propulsion Symposium, Chemical Propulsion Information Agency, 1999.

Shapiro, Ascher H. *The Dynamics and Thermodynamics of Compressible Fluid Flow*. New York: The Ronald Press Company, 1953.

Striebich, R. C. and W. A. Rubery, "Analytical Method for the Detection of Dissolved Oxygen," *Symposium on Distillate Fuel Auto-Oxidation Chemistry*, San Diego CA, March 1994.

Tucker, K. Colin, Paul I. King , Frederick R. Schauer and John L. Hoke. "Branched Detonation in a Multi-Tube PDE," ISABE 2003-1218, XVI International Symposium on Air Breathing Engines, 31 August – 5 September 2003, Cleveland OH.

Tucker, K. Colin, Paul I. King, Royce P. Bradley and Frederick R. Schauer. "The Use of a Flash Vaporization System with Liquid Hydrocarbon Fuels in a Pulse Detonation Engine," AIAA 2004-0868, 41st AIAA Aerospace Sciences Meeting & Exhibit, 5-8 January 2004, Reno NV.

Turns, Stephen R. *An Introduction to Combustion: Concepts and Applications*. New York: McGraw Hill, 2000.

White, Frank M. *Viscous Fluid Flow*. New York: McGraw Hill, 1991.

Vita

1st Lt Kristin L. Panzenhagen graduated from Robert E. Lee High School in Springfield, Virginia in June 1996. She attended Purdue University in West Lafayette, Indiana, where she graduated with a Bachelor of Science degree in Aeronautical Engineering in May 2000. She was commissioned through the Detachment 220 AFROTC at Purdue and recognized as a Distinguished Graduate.

She began active duty as a maintenance officer in the 1st Fighter Wing, Langley AFB, Virginia. At Langley, she served as Avionics Fight Commander, Accessories Flight Commander and Section Commander in the 1st Component Repair Squadron. In October 2001, she moved to the 71st Fighter Squadron, where she was the Assistant Sortie Generation Flight Commander. With the 71st, she participated in the Weapons Instructor Course at Nellis AFB, Nevada and the Weapons System Evaluation Program at Tyndall AFB, Florida. She deployed to Prince Sultan AB, Saudi Arabia from December 2001 through March 2002 in support of Operation Southern Watch. In September 2002, she entered the Air Force Institute of Technology Graduate School of Engineering and Management. Upon graduation, she will be assigned to the Air Vehicles Directorate of the Air Force Research Labs.

REPORT DOCUMENTATION PAGE

Form Approved
OMB No. 074-0188

1. REPORT DATE *(DD-MM-YYYY)*	2. REPORT TYPE	3. DATES COVERED *(From – To)*
23-03-2004	**Master's Thesis**	Sep 02 – Mar 04

4. TITLE AND SUBTITLE

DETONATION BRANCHING IN A PDE WITH LIQUID HYDROCARBON FUEL

5a. CONTRACT NUMBER

5b. GRANT NUMBER

5c. PROGRAM ELEMENT NUMBER

6. AUTHOR(S)

Panzenhagen, Kristin L., 1st Lt, USAF

5d. PROJECT NUMBER

5e. TASK NUMBER

5f. WORK UNIT NUMBER

7. PERFORMING ORGANIZATION NAMES(S) AND ADDRESS(S)

Air Force Institute of Technology
Graduate School of Engineering and Management (AFIT/ENY)
2950 Hobson Way
WPAFB OH 45433-7765

8. PERFORMING ORGANIZATION REPORT NUMBER

AFIT/GAE/ENY/04-M13

9. SPONSORING/MONITORING AGENCY NAME(S) AND ADDRESS(ES)

AFRL/PRTC
Attn: Dr. Fred Schauer
1790 Loop Road
WPAFB OH 45433-7765
DSN: 785-6462
e-mail: frederick.schauer@wpafb.af.mil

10. SPONSOR/MONITOR'S ACRONYM(S)

11. SPONSOR/MONITOR'S REPORT NUMBER(S)

12. DISTRIBUTION/AVAILABILITY STATEMENT

APPROVED FOR PUBLIC RELEASE; DISTRIBUTION UNLIMITED.

13. SUPPLEMENTARY NOTES

Advisor: Dr. Paul King, (937)255-3636, ext 4628 paul.king@afit.edu

14. ABSTRACT

A pulse detonation engine (PDE) capitalizes on the large mass flux and pressure rise associated with detonations to create thrust, which is proportional to PDE cycle frequency. This research showed that using a branched detonation as an ignition source, as opposed to standard spark ignition, deposits more energy into the thrust tube head. The increase in energy decreases ignition delay and detonation to deflagration transition (DDT) time. This allows a theoretical 85% cycle frequency increase that is accompanied by an 85% increase in thrust. The increase in energy also reduces the need for a DDT enhancement device, thereby increasing thrust as much as 30%. While detonation branching has been accomplished using gaseous hydrogen, this was the first instance of detonation branching using liquid hydrocarbon fuel.

15. SUBJECT TERMS

pulse detonation engine, detonation branching, ignition delay, detonation to deflagration transition

16. SECURITY CLASSIFICATION OF:			17. LIMITATION OF ABSTRACT	18. NUMBER OF PAGES	19a. NAME OF RESPONSIBLE PERSON
a. REPORT	b. ABSTRACT	c. THIS PAGE			Dr. Paul I. King
U	**U**	**U**	**UU**	90	19b. TELEPHONE NUMBER *(Include area code)* (937)785-3636, ext 4628; e-mail: paul.king@afit.edu